Applied Energy, Volume 230, Issue November, 2018, pp. 241-256
DOI: 10.1016/j.apenergy.2018.08.118

Feasibility of CaO/CuO/NiO sorption-enhanced steam methane reforming integrated with solid-oxide fuel cell for near-zero-CO_2 emissions cogeneration system

Giuseppe Diglio[a], Piero Bareschino[a,*], Erasmo Mancusi[a,*], Francesco Pepe[a], Fabio Montagnaro[b], Dawid P. Hanak[c], Vasilije Manovic[c]

[a]Dipartimento di Ingegneria, Università degli Studi del Sannio,
Piazza Roma 21, 82100 Benevento, Italy

[b]Dipartimento di Scienze Chimiche, Università degli Studi di Napoli Federico II,
Complesso Universitario di Monte Sant'Angelo, 80126 Napoli, Italy

[c]Clean Power Engineering, Energy and Power, School of Water, Energy and Environment,
Cranfield University, Cranfield MK43 0AL, United Kingdom

*Corresponding Authors: piero.bareschino@unisannio.it (P. Bareschino)
erasmo.mancusi@unisannio.it (E. Mancusi)

Abstract

In this article, a process for sorption-enhanced steam methane reforming in an adiabatic fixed-bed reactor coupled with a solid oxide fuel cell (SOFC) is evaluated using a 1D numerical reactor model combined with a simplified fuel cell simulation. A novel material comprising $CaO/CuO/Al_2O_3(NiO)$ pellets is considered. Three operating stages are considered in the proposed system, namely (i) CaO carbonation/reforming, (ii) Cu and Ni oxidation, and (iii) $CaCO_3$ calcination/CuO and NiO reduction. The operating conditions that enable cyclic operation of these stages and the strategy needed to switch between each stage are evaluated. Under the adopted control strategy, methane conversion was about 95%, whilst H_2 yield and purity were around 3.2 mol_{H2} mol_{CH4}^{-1} and 90%, respectively. Moreover, a concentrated CO_2 stream ready for storage was obtained. By using a portion of the produced H_2 to make the process self-sufficient from an energy standpoint, an equivalent H_2 yield and a reforming efficiency of about 2.8 mol_{H2} mol_{CH4}^{-1} and 84% were achieved, respectively. With respect to SOFC integration, net power and thermal energy generation of around 11 kW and 6 kW, respectively, can be achieved. With respect to the chemical energy of the inlet methane, the net electrical and thermal efficiencies of the considered process are 56% and 30%, respectively, *i.e.*, the overall efficiency of the entire system is 86%. The proposed cogeneration system showed better thermodynamic, environmental and economic performances than those of conventional systems, with an investment pay-back period of 2.2 years in the worst-case scenario. The levelised cost of electricity, of heat and total power were about 0.096 € kWh^{-1}, 0.19 € kWh^{-1}, and 0.065 € kWh^{-1}, respectively, while the CO_2 emissions were avoided at no cost.

Keywords: CO_2 capture; Oxygen carrier and catalyst; Hydrogen production; Solid Oxide Fuel Cell; Cogeneration.

Nomenclature

A	Cross-section area, m^2
AC	Cost of CO_2 avoided, € t_{CO2}^{-1}
B_{H2}	Standardised amount of H_2 produced per mass of CaO in the bed, kg_{H2} kg_{CaO}^{-1}
CF	Capacity factor, -
C_i	Concentration of species *i*, mol m^{-3} (gas species and Cu solid species), kg kg^{-1} (C and Ni solid species)
$CO_{2,SE\text{-}SMR}$	Mass of CO_2 at the outlet of SE-SMR during single $CaCO_3$ calcination stage, t_{CO2}
CO_{2equiv}	Equivalent CO_2 emissions, t_{CO2} y^{-1}
COP	Coefficient of performance, -
cp	Heat capacity, J kg^{-1} K^{-1}
CTS	CO_2 transport and storage cost, € t_{CO2}^{-1}
d	Diameter, m
D_{ax}	Axial dispersion coefficient, m^2 s^{-1}
DEN	Denominator of reforming reaction rates
d_{cell}	Diameter of cell, m
$d_{HE/cond}$	Heat exchanger/condenser tube outer diameter, m
e_{CO2}	Specific CO_2 emission, t_{CO2} kWh^{-1}
E_{el}	Electric power, W
E_{th}	Thermal power, W
E_{tot}	Total power, W
E_W	Heat losses through reactor wall, W
F	Faraday constant, A, s mol^{-1}
f	Design stress of carbon steel, bar
FCF	Fixed charge factor, y^{-1}
fu	Fuel cell fuel utilisation factor, -
G	Mass flux of the gas phase, kg m^{-2} s^{-1}
h	Hours in year, h/y
H_{ext}	External heating and power demand, J mol_{CH4}^{-1}
IC	Investment cost, €
k	Ideal gas specific heat ratio, -

L	Reactor length, m
L_{cell}	Cell length, m
LCOE	Levelised cost of electricity, € kWh^{-1}
LCOH	Levelised cost of heat, € kWh^{-1}
LCOTP	Levelised cost of total power generation, € kWh^{-1}
$L_{HE/cond}$	Length of heat exchanger/condenser tube, m
LHV	Lower heating value, J mol^{-1}
M	Molecular weight, kg mol^{-1}
MC	Yearly (hourly) maintenance cost, € y^{-1} (€ h^{-1})
m_f	Mass flow rate, kg s^{-1}
M_{sol}	Mass of solid in the bed, kg
n	Molar flow rate, mol s^{-1}
$n_{u,cells}$	Number of cells, -
$n_{u,HE/cond}$	Number of heat exchanger/condenser tubes, -
OC	Fixed and variable operating cost, € y^{-1}
P	Pressure, bar
P_0	Standard pressure, bar
PE	Primary energy input per annum, kWh
P_i	Partial pressure of species *i*, bar
Q	Gas volumetric flow rate, m^3 s^{-1}
R_g	Ideal gas constant, J mol^{-1} K^{-1}
r_i	Rate of consumption or formation of species *i*, mol m^{-3} s^{-1}
r_{RJ}	Rate of reaction *j* per unit volume of the oxygen carrier, mol m^{-3} s^{-1}
sc	Specific cost, € kg^{-1}, € m^{-2}, € m^{-3} or € kW^{-1}
S_{H2}	H_2 purity, %
s_{refr}	Thickness of refractory, m
s_s	Thickness of the steel vessel, m
T	Temperature, K
t	Time, s
TCR	Total capital requirement, €
u	Gas superficial velocity, m s^{-1}
UP	Unit price, € kWh^{-1}
V_{loss}	Fuel cell voltage loss, V
Vol	Volume, m^3

V_{SOFC}	SOFC voltage, V
w	Solid mass fraction, -
X	Solid conversion degree, -
x_{CH4}	Methane conversion, %
X_{max}	Maximum sorbent conversion, -
y_i	Molar fraction of gas species *i*, -
z	Axial spatial variable, m

Greek letters

α	Stoichiometric coefficient of carbon oxidation reaction, -
β	Partition ratio, -
γ	Efficiency, -
ΔG^0_f	Change in molar Gibbs free energy of formation, J mol^{-1}
$\Delta H_{\square}$	Enthalpy of reaction j, J mol^{-1}
$\varepsilon_{\square}$	Solid void fraction, -
λ	Thermal conductivity of refractory, W m^{-1} K^{-1}
$\lambda_{\alpha\xi}$	Axial heat dispersion coefficient, W m^{-1} K^{-1}
ι	H_2 partition ratio, -
μ	Specific emission factor, kg_{CO2} kWh^{-1}
Π	Period, s
ρ	Density, kg m^{-3}
σ	Effectiveness factor, -
υ	Volume fraction, -
ψ_{H2}	H_2 yield, mol_{H2} mol_{CH4}^{-1}

Subscripts

0	Initial
a	Refractory and reactor
act	Initial active phase
amb	Ambient
aux	Auxiliaries
B	Boiler
c	Carrier/Catalyst
comp	Compressor

cs	Conventional system
ee	Electric energy
el	Electric
eq	Equilibrium
equiv	Equivalent
f	Feed
g	Gas
HE/cond	Heat exchanger/condenser
i	Solid and gas species (Cu, Ni, C, CH_4, H_2, H_2O, CO, CO_2, O_2, N_2)
in	Inlet
inv	Inverter
j	Chemical reaction index
k	Stage index (CAR, OX and CAL)
max	Maximum
net	Net
NG	Natural gas
out	Outlet
p	Particle
ps	Proposed system
r	Reactor
ref	Reforming
refer	Reference
refr	Refractory
s	Sorbent
sol	Solid material
stack	Fuel cell stack
th	Thermal
tot	Total
V	High-temperature valve
y	Solid compounds (Cu, Ni, CaO)

Acronyms

ATR	Auto-Thermal methane Reforming
CAL	$CaCO_3$ CALcination/CuO and NiO reduction stage

CAR	Reforming/CaO CARbonation stage
CLR	Chemical Looping Reforming
EG	Electric Grid
EHP	Electric Heat Pump
FESR	Fuel Energy Saving Ratio
MCHP	Micro Combined Heat and Power
OX	Cu and Ni OXidation stage
PS	Purge Stage
SE-SMR	Sorption-Enhanced Steam Methane Reforming
SMR	Steam Methane Reforming
SOFC	Solid Oxide Fuel Cell

1. Introduction

In 2015 the world total primary energy consumption was about $1.62 \cdot 10^4$ GWh, 80% of which was supplied from fossil fuels. Consequently, around 32 Gt of CO_2, 42% of which corresponded to electricity and heat generation [1], was released to the atmosphere [2]. In a business-as-usual scenario, this number is expected to grow to about 48 Gt/year by 2040 [3]. In this context, attempts are being undertaken to ensure a timely transition towards hydrogen-based energy systems, at the expense of conventional fossil fuel-based systems, and high-efficiency energy-conversion devices like fuel cells [4]. However, since H_2 is a secondary form of energy that has to be produced, it should be as environmentally friendly as the system used for its production.

Steam Methane Reforming (SMR) and Auto-Thermal methane Reforming (ATR) are the most commonly used systems at the moment, while Chemical Looping Reforming (CLR) is currently considered as one of the most promising technologies for low-carbon hydrogen production [5]. In both SMR and ATR a mixture of methane and steam is fed to a packed-bed reactor filled with a Ni-based catalyst. In the former system, the heat required to drive the endothermic reforming reactions is supplied by an external furnace. In the latter system, O_2 is fed simultaneously with fuel and steam, tailoring the operating conditions in such a way as to reach thermal equilibrium between combustion and reforming reactions [6]. On the contrary, CLR is a cyclic process based on a Ni-based metal oxide acting not only as oxygen carrier, but also as a catalyst for the reforming reactions. In such a system two stages can be distinguished: an oxidation stage in which the carrier is oxidised by feeding air to the reactor, and a reduction stage in which fuel and steam are fed to the reactor both to reduce the solid material and to carry out reforming reactions [7]. CLR is generally operated in a dual fluidised bed configuration in which the carrier/catalyst is constantly circulated between an air reactor, where the oxidation reaction takes place, and a fuel reactor, where reduction reactions occur. However, other researchers have favoured fixed beds for CLR [8]. The main drawback of the aforementioned processes is the need of a downstream purification system comprising, at least, one water gas shift reactor to boost the H_2 content in the produced syngas, and one CO_2 separation unit. Even in the simplified configuration, the H_2 enrichment stage is the most expensive section and increases the complexity of the entire system [9].

Sorption-Enhanced Steam Methane Reforming (SE-SMR) represents an attractive alternative to overcome this issue [10]. The key element of this process is the solid material that can be seen as a mixture of reforming catalyst (Ni) and CaO, which is the most commonly used solid sorbent for

CO_2 capture [11]. While the first component enhances the reforming reactions, the second reacts with the CO_2 produced during the reforming process *via* the carbonation reaction, producing $CaCO_3$. The effluent gas is a high-purity H_2 stream (~ 90%) [12]. The solid sorbent is then regenerated through the $CaCO_3$ calcination reaction, yielding a stream of concentrated CO_2. Although the reforming/carbonation stage is an autothermal process, as the endothermic H_2 production step is driven by the exothermic CO_2 adsorption, the heat needed to carry out the endothermic calcination step is the main obstacle to large-scale deployment of SE-SMR [13]. Many attempts were undertaken to address this engineering challenge. Antzara *et al*. [14] experimentally demonstrated that heat required by the calcination step can be supplied by an exothermic Ni oxidation step. In this case, a subsequent Ni reduction step should be carried out. Barelli *et al*. [15] experimentally evaluated the performance of sorbent material based on incorporation of CaO particles into calcium aluminates, finding that this material is characterised by lower regeneration temperature than conventional CaO. Recently, a novel CaO-based sorbent was developed by mechanical mixing with Cu-based oxygen carrier and Ni-based catalyst [16] ($CaO/CuO/Al_2O_3(NiO)$). SE-SMR processes carried out using this novel catalyst can be divided into three steps, namely i) the reforming/CaO CARbonation stage (CAR); ii) Cu and Ni OXidation stage (OX); and iii) $CaCO_3$ CALcination/CuO and NiO reduction stage (CAL), so that the endothermic $CaCO_3$ calcination step can be driven *via* the heat generated by the exothermic CuO reduction reaction. SE-SMR chemical looping processes were investigated both experimentally and by means of numerical simulations. Qin *et al*. [17] experimentally determined kinetic parameters of CuO reduction and sorbent regeneration reactions, and subsequently incorporated them into an adiabatic fixed-bed mathematical model to simulate the calcination stage, finding that the operating temperature is the key parameter to avoid local hot spots in the reactor. Fernandez *et al*. [18] experimentally tested (in a lab-scale fixed-bed reactor) and numerically simulated the $CaCO_3$ calcination/CuO and NiO reduction stage using a pseudo-homogeneous reactor model, considering H_2 as reducing gas. They found that a Cu/Ca molar ratio of 1.8 enabled both the CuO reduction and sorbent regeneration reaction fronts to advance jointly, reaching a maximum temperature in the bed of about 1143 K. Tan *et al*. [19] synthesised a NiO/CuO composite and experimentally tested its catalytic activity for H_2 production. Diez-Martin *et al*. [20] experimentally investigated the reduction reaction kinetics with hydrogen, carbon monoxide and methane of two high-load CuO-based materials with different supports for Ca/Cu looping processes. They found that the reduction reaction was kinetically controlled for the Al_2O_3-supported material, while the internal diffusion resistance becomes predominant for the $MgAl_2O_4$-supported one. San Pio *et al*. [21] experimentally verified that the total pressure has no influence on the reduction reaction of CuO-based oxygen carrier used for SE-SMR chemical looping processes. San Pio *et al*. [22] numerically

studied dynamically-operated packed-bed reactors filled with CuO/Al_2O_3 oxygen carrier for chemical looping systems and pointed out that including the formation and reduction kinetics of spinel compounds ($CuAl_2O_4$ and $CuAlO_2$) is of paramount importance to predict reactor performance. Garcia-Lario *et al*. [23] demonstrated experimentally and numerically that both H_2 and CO enhance reduction reactions of high-load CuO-based material for Ca/Cu chemical looping. Using a 1D pseudo-homogeneous mathematical model, Fernandez *et al*. [24] analysed the performance of ($CaO/CuO/Al_2O_3$(NiO)) pellets in the reforming/CaO carbonation stage, which took place in an adiabatic fixed bed, in terms of methane conversion, H_2 yield and CO_2 capture level. That study evaluated the effect of catalyst/sorbent ratio, operating temperature, operating pressure and steam-to-carbon feed ratio and showed a maximum H_2 purity of about 96% at an operating pressure of 35 bar and steam-to-carbon feed ratio of 6. Additionally, it was shown that H_2 production is favoured at operating temperatures above 973 K. Alarcon and Fernandez [25] numerically carried out a sensitivity analysis on the feasibility of $CaCO_3$ calcination/CuO and NiO reduction stages in an adiabatic fixed-bed reactor by changing copper/sorbent molar ratio, bed initial temperature and fuel gas composition. They highlighted that all these parameters should be carefully selected in order to achieve a complete reduction and regeneration of the oxygen carrier and sorbent, respectively, and to prevent copper thermal deactivation. Martini *et al*. [26] studied CAR, OX and CAL stages separately, by means of a simplified model based on a reaction front approach. The aim was to find process operability windows of such stages. It is important to highlight here that they did not evaluate the cyclic performance of the SE-SMR process considering several CAR, OX and CAL cycles. In a further development of their work, Martini *et al*. [27] numerically investigated the influence of different operating parameters on the performance of the reforming/CaO carbonation stage by means of a 1D pseudo-homogeneous reactor model integrating a simplified reaction kinetic scheme.

On the basis of the above-cited literature it appears that, although several papers can be found dealing with modelling and simulation of CaO carbonation, Cu oxidation and $CaCO_3$ calcination/CuO reduction stages, $CaO/CuO/Al_2O_3$(NiO)-catalysed SE-SMR still poses a number of unsolved challenges. In particular, to the best of the authors' knowledge, no study presented in the published literature:

I. studied the complete cyclic SE-SMR process based on $CaO/CuO/Al_2O_3$(NiO) solid material;
II. proposed an integration between a $CaO/CuO/Al_2O_3$(NiO)-catalysed SE-SMR system with a solid oxide fuel cell as a near-zero-CO_2 emissions cogeneration system;
III. assessed the techno-economic feasibility of such integration.

This paper numerically addresses the above points with the aim of supporting both the transition towards H_2-based energy cogeneration systems and the commercialisation of such processes. In particular, the dynamic behaviour of an adiabatic fixed-bed reactor in which CAR, OX and CAL stages cyclically follow each other was numerically investigated. Although recent theoretical studies deal with numerical simulation of $CaO/CuO/Al_2O_3$(NiO)-catalysed SE-SMR processes, no paper has considered complex kinetic schemes. In this work, to the best of the authors' knowledge, all reactions between gaseous and solid phases have been accounted for. The cyclic behaviour of $CaO/CuO/Al_2O_3$(NiO) pellets, when used in Ca/Cu looping, is comprehensively investigated by evaluation of both the operating conditions to cyclically couple CAR, OX and CAL and the strategy required to switch between each stage in order to maximise both H_2 yield and reforming efficiency.

Moreover, the coupling between the proposed SE-SMR system and a solid oxide fuel cell is discussed in order to propose a near-zero-CO_2 emissions high-efficiency cogeneration system, following Barelli *et al.* [28]. Finally, the comparison of such integration to conventional cogeneration systems is assessed, as well as its techno-economic feasibility.

2. Mathematical model

2.1 Kinetic scheme

The reactions of interest and the corresponding standard reaction enthalpies are reported in Tab. 1. During the reforming/CaO carbonation stage, steam methane reforming (SMR - R1), water gas shift (WGS - R2), overall steam methane reforming (OSMR - R3), methane decomposition (R4), carbon gasification by steam (R5) and by CO_2 (R6) and CaO carbonation reaction (R7) were considered. The reaction mechanism proposed by Xu and Froment [29] was considered to describe SMR, WGS and OSMR, while those proposed by Iliuta *et al*. [30] and Rodriguez *et al*. [31] were employed for R4, R5, R6 and R7. CO_2 partial pressure was expressed according to Baker [32]. During the Cu and Ni oxidation stage, the oxidation reactions of Cu (R8), Ni (R9) and carbon deposited onto the carrier surface (R10) were accounted for.

Table 1 - Global reactions and associated standard reaction enthalpies implemented in the mathematical model.

Reaction	ΔH^0, kJ·mol^{-1}	
Reforming/CaO Carbonation stage		
$CH_4 + H_2O \xrightarrow{Ni} CO + 3H_2$	206	R1
$CO + H_2O \xrightarrow{Ni} CO_2 + H_2$	-41	R2
$CH_4 + 2H_2O \xrightarrow{Ni} CO_2 + 4H_2$	165	R3
$CH_4 + Ni \xrightarrow{Ni} Ni - C + 2H_2$	74	R4
$C + H_2O \xrightarrow{Ni} CO + H_2$	131	R5
$C + CO_2 \xrightarrow{Ni} 2CO$	172	R6
$CaO + CO_2 \rightarrow CaCO_3$	-179	R7
Cu and Ni Oxidation stage		
$2Cu + O_2 \rightarrow 2CuO$	-312	R8
$2Ni + O_2 \rightarrow 2NiO$	-479	R9
$C + \left(\frac{1+\alpha}{2}\right) O_2 \rightarrow \alpha CO_2 + (1-\alpha) CO$	[-787, -110]	R10
CuO and NiO Reduction/$CaCO_3$ Calcination stage		
$4CuO + CH_4 \rightarrow 4Cu + CO_2 + 2H_2O$	-178	R11
$CuO + CO \rightarrow Cu + CO_2$	-127	R12
$2CuO + 2H_2 \rightarrow 2Cu + 2H_2O$	-86	R13
$2NiO + CH_4 \rightarrow 2Ni + 2H_2 + CO_2$	161	R14
$NiO + CO \rightarrow Ni + CO_2$	-43	R15
$NiO + H_2 \rightarrow Ni + H_2O$	-2	R16
$NiO + CH_4 \rightarrow Ni + 2H_2 + CO$	203	R17
$CaCO_3 \rightarrow CaO + CO_2$	179	R18

The Cu oxidation reaction was modelled using the kinetic expression proposed by Garcia-Labiano *et al.* [33], while that reported by Dueso *et al.* [34] was used to describe Ni oxidation. The kinetic expression reported by Hurt and Calo [35] was considered for the carbon oxidation reaction. Both partial and complete carbon oxidation were accounted for, according to the stoichiometric coefficient α [35] (for symbols please see the nomenclature). During the CuO and NiO reduction/$CaCO_3$ calcination stage, the kinetics of Cu reduction with CH_4 (R11), CO (R12) and H_2 (R13) reported by Garcia-Labiano *et al.* [33] were considered. Partial CH_4 oxidation (R14 and R17), CO (R15) and H_2 (R16) oxidation were taken into account for Ni, whose reaction rates were expressed according to Iliuta *et al.* [30]. The reaction mechanism proposed by Martinez *et al.* [36] was considered for the calcination reaction (R18).

2.2 Mass and energy balance

A one-dimensional adiabatic fixed-bed pseudo-homogeneous model was used to study the cyclic behaviour of the SE-SMR process. The absence of radial concentration and temperature

gradients, as well as the lack of interphase concentration and temperature gradients and intra-particle temperature gradients, were checked following the approach of Diglio *et al*. [13] (details not reported here for the sake of brevity). Following Fernandez *et al*. [37], to consider that intra-particle concentration gradient effects could be limiting for the overall reaction scheme, all kinetic constants were scaled by means of an effectiveness factor(σ= 0.3) with the exception of the calcination reaction (σ = 1), for which the temperature is the main limiting parameter. The other model assumptions are: (a) ideal gas behaviour; (b) uniform particle size of solid material; and (c) perfect mixing of the oxygen carrier, catalyst and sorbent. As reported by Antzara *et al*. [38], the CO_2 adsorption capacity of the sorbent decreases after a few carbonation/calcination cycles; after that, an almost constant value over around 50 subsequent cycles is assumed. To take the decay in CO_2 adsorption capacity into account, the approach suggested by Fernandez *et al*. [37] was adopted, by assuming a maximum sorbent adsorption capacity of 40% of its nominal value (X_{max} = 0.4). The model equations for CAR, OX and CAL are reported in Tab. 2. The axial dispersion coefficient (D_{ax}) was evaluated according to the correlation proposed by Edwards and Richardson [39], while the one reported by Yagi and Wakao [40] was taken into account for the effective heat dispersion coefficient (λ_{ax}).

Table 2 - Mathematical model.

Mass balance in the gas phase

$$\left(1-\varepsilon_s\right)\frac{\partial C_i}{\partial t}+\frac{\partial\left(uC_i\right)}{\partial z}=\left(1-\varepsilon_s\right)\frac{\partial}{\partial z}\left(D_{ax}\frac{\partial C_i}{\partial z}\right)+\sigma\varepsilon_s r_i$$

Energy balance

$$\left[\varepsilon_s\rho_{sol}cp_{sol}+\left(1-\varepsilon_s\right)\rho_g cp_g\right]\frac{\partial T}{\partial t}+\frac{\partial\left(u\rho_g cp_g T\right)}{\partial z}=\left(1-\varepsilon_s\right)\frac{\partial}{\partial z}\left(\lambda_{ax}\frac{\partial T}{\partial z}\right)+\sigma\varepsilon_s\sum_j r_{Rj}\Delta H_{Rj}$$

Momentum equation

$$\frac{dP}{dz}=-10^{-5}\left[\frac{150\mu_g\left(1-\varepsilon_s\right)^2}{d_p^2\varepsilon_s^3}u+\frac{1.75\left(1-\varepsilon_s\right)}{d_p\varepsilon_s^3}\rho_g u^2\right]$$

Solid mass balance

$$\frac{\partial C_{Cu}}{\partial t}=r_{Cu},\quad \frac{\partial C_{Ni}}{\partial t}=\frac{r_{Ni}}{\rho_c}M_{Ni},\quad \frac{\partial C_C}{\partial t}=\frac{r_C}{\rho_c}M_C$$

	CAR	OX	CAL
Cu conversion degree	$\frac{\partial X_{Cu}}{\partial t}=0$	$\frac{\partial X_{Cu}}{\partial t}=-\frac{\sigma}{\rho_{Cu}}\frac{r_{Cu}}{C_{CuO,max}}$	$\frac{\partial X_{Cu}}{\partial t}=\frac{\sigma}{\rho_{Cu}}\frac{r_{Cu}}{C_{CuO,max}}$
Ni conversion degree	$\frac{\partial X_{Ni}}{\partial t}=0$	$\frac{\partial X_{Ni}}{\partial t}=-\frac{\sigma}{\rho_c}r_{Ni}\frac{W_{Ni}}{M_{NiO}}$	$\frac{\partial X_{Ni}}{\partial t}=\frac{\sigma}{\rho_c}\frac{r_{Ni}}{C_{NiO,max}}$
CaO conversion degree	$\frac{\partial X_s}{\partial t}=\sigma r_{Rf}\frac{M_{CaO}}{\rho_s}$	$\frac{\partial X_s}{\partial t}=0$	$\frac{\partial X_s}{\partial t}=-\sigma r_{Rf8}\frac{M_{CaCO_3}}{\rho_s}$

Assuming that the process starts with the reforming/CaO carbonation stage, the first-run-only initial condition for the CAR of the very first cycle is expressed as:

$$\begin{cases} C_{CH_4}(z,0) = C_{H_2}(z,0) = C_{H_2O}(z,0) = C_{CO}(z,0) = C_{CO_2}(z,0) = C_{O_2}(z,0) = C_{N_2}(z,0) = C_C(z,0) = 0 \\ C_{Cu}(z,0) = C_{Cu,max} \\ C_{Ni}(z,0) = w_{Ni} \\ X_{Cu}(0) = X_{Ni}(0) = 1 \\ X_s(0) = 0 \\ T(z,0) = T_0 \\ P(z,0) = P_{CAR/OX} \end{cases} \quad (1)$$

The initial conditions for subsequent stages were taken from the last computed values from the previous stage, according to the cyclic nature of the SE-SMR process. Further details on the mathematical expression of initial cyclic conditions can be found in [13].

For both the mass balance in the gas phase and the energy balance, Danckwerts (Langmuir) and Neumann boundary conditions were used while a Dirichlet boundary condition was implemented for the momentum equation. Model parameters used in the simulations are reported in Tab. 3. Reactor parameters (L, d_r and ε_s) were taken from Noorman *et al*. [8], while temperature and pressure inlet and initial conditions (T_f, T_0, $P_{CAR/OX}$ and P_{CAL}), as well as H_2O-to-CH_4 feed ratio during CAR, were selected from Fernandez *et al*. [37] and Alarcon and Fernandez [18]. As assessed by Qin *et al*. [17], over OX an inlet temperature ($T_{f,CAL}$) higher than that of the remaining stage is required in order to promote the calcination reaction. The mass flux of the gas phase during the reforming/CaO carbonation stage ($G_{CAR/CAL}$) was assumed from Noorman *et al*. [8], while the one in the Cu and Ni oxidation stage (G_{OX}) was assessed to reach a superficial velocity of about 0.5 m s^{-1}, which is close to the normal range of operation in industrial SMR systems [41]. Solid compound mass fractions (w_{CaO}, w_{Cu}, $w_{Al2O3(NiO)}$ and w_{Ni}) were taken from [13], while the density of solid material (ρ_{sol}) and maximum Cu concentration ($C_{Cu,max}$) were assumed according to Garcia-Labiano *et al*. [33].

For the evaluation of temperature, pressure and composition dependencies of reaction enthalpies, transport coefficient and gas properties, state-of-the-art correlations and assumptions were adopted from Han *et al*. [42] and references therein.

The mathematical model was solved using the commercial software Comsol Multiphysics®. Reactor length (L) was discretised with 500 nodes and it was verified that further refinements of the spatial mesh do not produce any appreciable changes in the calculated temperature and concentration profiles. Validation of the above-described mathematical model against literature data was discussed elsewhere [7,13,43,44].

Table 3 - Parameters used in the simulations.

Reactor length, L	1 m
Reactor diameter, d_r	0.05 m

Particle diameter, d_p	0.01 m
Solid void fraction, ε_s	0.5
Feed temperature during carbonation and oxidation stage, $T_{f,CAR/OX}$	1073 K
Feed temperature during calcination stage, $T_{f,CAL}$	1150 K
Initial temperature of the bed, T_0	1073 K
Pressure during carbonation and oxidation stage, $P_{CAR/OX}$	35 bar
Pressure during calcination stage, P_{CAL}	1 bar
H_2O-to-CH_4 molar feed ratio during CAR	5
Mass flux of the gas phase in CAR and CAL, $G_{CAR/CAL}$	1 kg m^{-2} s^{-1}
Mass flux of the gas phase in OX, G_{OX}	10 kg m^{-2} s^{-1}
Mass fraction of sorbent, w_{CaO}	0.45
Mass fraction of copper, w_{Cu}	0.45
Mass fraction of alumina, $w_{Al2O3(NiO)}$	0.10
Mass fraction of nickel with respect to alumina, w_{Ni}	0.10
Density of solid material, ρ_{sol}	1632 kg m^{-3}
Mass of solid in the bed, M_{sol}	1.6 kg
Density of solid compound, ρ_y	$\rho_y = \frac{w_y M_{sol}}{\varepsilon_s Vol_r}$
Maximum Cu concentration, $C_{Cu,max}$	9225 mol m^{-3}

3. Results and discussion

3.1 Single reforming/CaO carbonation stage

Figure 1 reports the profiles for the main gas products coming from CAR, *i.e.*, (a) outlet H_2 and CO_2 molar fractions (dry basis) as functions of time, (b) sorbent spatial conversion degree profiles for five time points, and (c) outlet temperature during the first CAR cycle. By inspecting Fig. 1(a) three different stages can be detected, namely pre-breakthrough (blue), breakthrough (white) and post-breakthrough (red). Over the first stage, CO_2 is adsorbed *via* CaO carbonation (R7) resulting in a high-purity H_2 outlet gas stream (~92%). The remaining gas products are some unreacted CH_4 (~7%) and CO (~1%), the last not reported in Fig. 1(a) for the sake of clarity. Over this stage the standardised amount of hydrogen produced per mass of calcium oxide in the bed (B_{H2}) is about 0.11 kg_{H2} kg_{CaO}^{-1}. During the breakthrough stage, the purity of H_2 quickly decreases while y_{CO2} gradually increases (B_{H2} ~ 0.03 kg_{H2} kg_{CaO}^{-1}), since the sorbent adsorption capacity is approaching its saturation value as shown in Fig. 1(b) (see line at t = 750 s). Over the third stage, only reforming (R1, R2 and R3), methane decomposition (R4) and carbon gasification (R5 and R6) reactions occur since the sorbent is fully saturated (in Fig. 1(b), at t = 1500 s $X_s = X_{max}$ along the whole bed length), and H_2 and CO_2 concentrations reach their equilibrium values. Over this last stage B_{H2} is about 0.01 kg_{H2} kg_{CaO}^{-1}. Thus, considering the whole reforming/CaO carbonation stage, the value of the standardised amount of hydrogen produced per mass of calcium oxide in the bed is about 0.15 kg_{H2} kg_{CaO}^{-1}, which is close to the value given by Martini *et al.* [26].

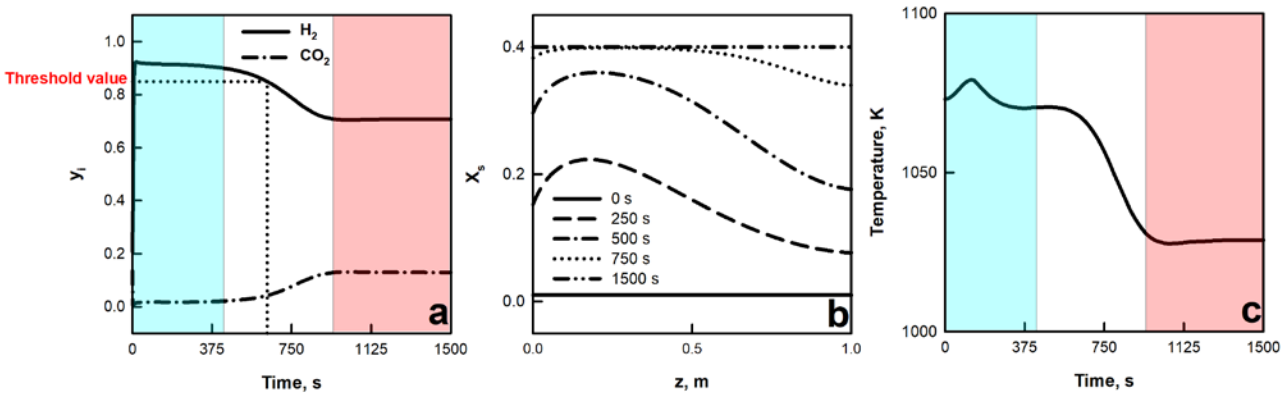

Figure 1 - Outlet H_2 and CO_2 molar fractions on dry basis as function of time (a), sorbent conversion degree at different time (b) and outlet temperature (c) during the first CAR cycle (pre-breakthrough stage in blue, breakthrough stage in white and post-breakthrough stage in red)

As shown in Fig. 1(c), the outlet gas temperature increases during the pre-breakthrough stage since the overall reaction occurring during CAR (from R1 to R7) is slightly exothermic. From the

breakthrough stage, the temperature decreases because the sorbent is becoming saturated and only globally endothermic reforming reactions (from R1 to R6) occur.

Importantly, the period of CAR strongly affects the purity of produced H_2: in order to maximise the H_2 content in the gas stream while removing as much CO_2 as possible, the CAR period should be no longer than the breakthrough stage (see Fig. 1(a) – blue and white zones). In this case a hydrogen breakpoint value of 85% was chosen as the switching condition, *i.e.*, the controller dictates the switch from CAR to OX when the outlet H_2 molar fraction reaches the threshold value of 0.85. Any further extension of CAR, while increasing the CaO carbonation degree, would have the detrimental effect of quickly reducing the H_2 purity. Notably, given the amount of steam in the feed, catalyst fouling due to carbon deposition does not occur.

3.2 Single Cu and Ni oxidation stage

The main scope of this stage is to oxidise the Cu present in the solid material in order to drive, in the subsequent CAL, the endothermic calcination reaction *via* the heat released by CuO reduction reactions. The operating conditions over OX should be carefully tailored in order to enhance the kinetics of the Cu oxidation reaction and to avoid $CaCO_3$ calcination. The Cu oxidation reaction should be as fast as possible so as to decrease the OX period and, as a consequence, also the required reactor length for a given gas superficial velocity. For this reason, as reported by Fernandez *et al*. [45], OX should be operated at high pressure. At the same time, the calcination kinetics are not favoured at high pressure. The $CaCO_3$ calcination is an undesirable reaction during OX given that any CO_2 at the exit of the reactor would be diluted with nitrogen. Since CAR was carried out at 35 bar, the same pressure was chosen to run the OX stage. Calcination over OX can be further minimised by keeping the temperature in the reactor as low as possible. As suggested by Martini *et al*. [27], thermal-neutral conditions over OX can be achieved by feeding a lean oxygen-nitrogen mixture with an O_2 molar fraction of about 3% to the reactor. Such inlet conditions are reached by mixing part of the nitrogen leaving the reactor with air feed, with a N_2 recirculation ratio of 0.18, thereby also avoiding excessive overheating of the reactor that could lead to irreversible deterioration of the solid materials. It was verified that, after this mixing, the gas stream inlet temperature decreases less than 3 K. Figure 2 shows outlet O_2 and N_2 molar fractions as functions of time (a), Cu and Ni spatial conversion profiles for five time points (b), and outlet temperature (c), during the first OX stage. As reported in Fig. 2(a), the O_2 inlet concentration was chosen as the threshold value for the controller to dictate the switch from OX to CAL (the filled pattern in Fig. 2 represents the time window where the oxidation stage should no longer occur). Indeed, when the O_2 outlet molar fraction reaches its feeding value, both Cu and Ni are fully oxidised (see Fig. 2(b) line at t = 1600 s). The period of OX is linked to the

oxidation of Cu since, as depicted in Fig. 2(b), the velocity of the Ni oxidation front is slightly higher than that for Cu, as the Ni content in the solid material is lower. It is noteworthy that the maximum temperature reached in this stage (~1090 K) is quite close to the inlet value (1073 K), as shown in Fig. 2(c).

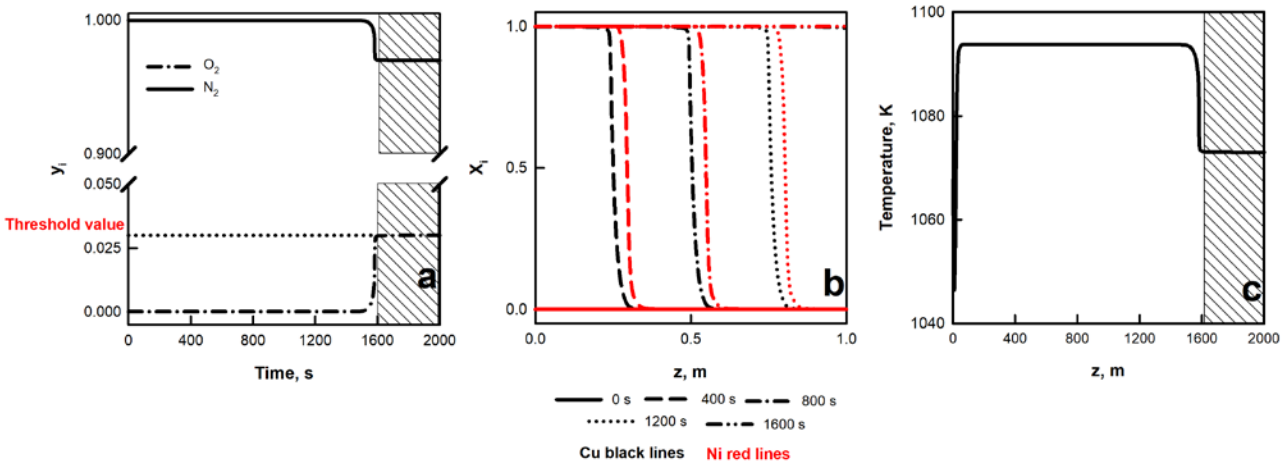

Figure 2 - Outlet O_2 and N_2 molar fractions as functions of time (a), Cu and Ni spatial conversion degree at different times (b), and outlet temperature (c), during the first OX cycle.

3.3 Single $CaCO_3$ calcination/CuO and NiO reduction stage

As reported by Alarcon and Fernandez [25], the operating conditions of CAL should be chosen in order to ensure that: i) the CuO reduction reaction front reaches the exit of the bed after $CaCO_3$ is fully calcined; ii) the heat released by the CuO reduction reaction is in balance with heat required by the endothermic $CaCO_3$ calcination and NiO reduction, to avoid either overheating inside the reactor or the need of external heating. Since the kinetics of the calcination reaction are favoured at low pressure, CAL is operated at atmospheric pressure. Since the $CaCO_3$/CuO ratio in the solid material is fixed, the reacting gas composition represents the only parameter that can be tailored to ensure the two aforementioned conditions. According to Qin *et al*. [17], by feeding a mixture of 30% CH_4 and 70% CO_2 to the reactor, such requirements can be satisfied. Fig. 3 reports the outlet CH_4 and CO_2 molar fractions (dry basis) as functions of time (a), sorbent, Cu and Ni spatial conversion degree profiles for four time points (b), and outlet temperature (c), during the first CAL stage.

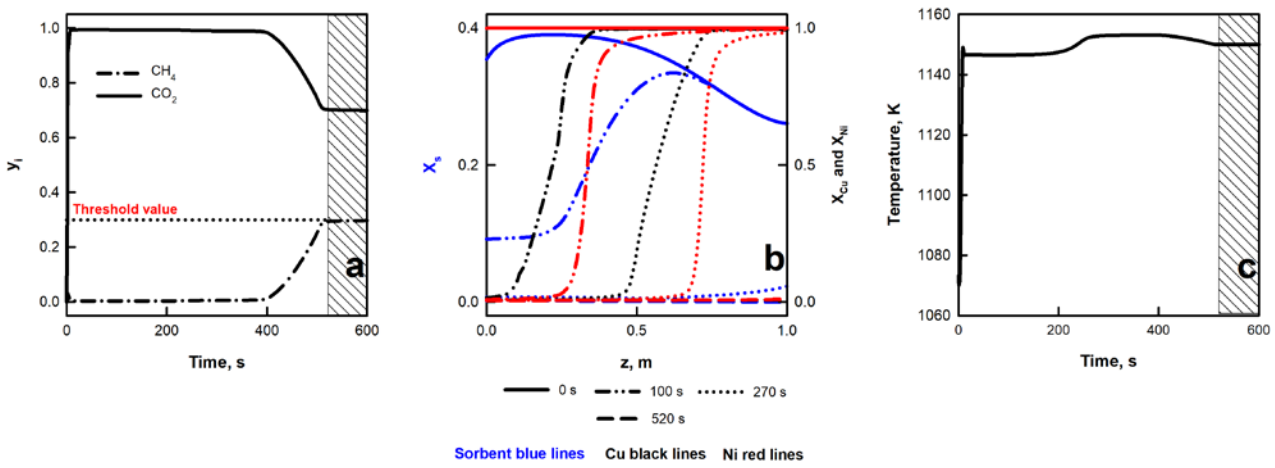

Figure 3 - Outlet CH_4 and CO_2 molar fractions (dry basis) as functions of time (a), sorbent, Cu and Ni spatial conversion degree at different times (b), and outlet temperature (c), during the first CAL cycle.

The controller dictates the switch from CAL to CAR when the outlet CH_4 molar fraction reaches its inlet value (see threshold value in Fig. 3(a)); thus, the filled pattern in Fig. 3 represents the time window that should be outside the calcination stage. In fact, at this time point both Cu and Ni in the solid material are fully oxidised (see line at t = 520 s in Fig. 3(b)). Importantly, CO_2 at the exit of the reactor over this stage can be easily separated by water through a condensation process and then recirculated to guarantee the desired inlet conditions. Again, as shown in Fig. 3(b), the Cu reduction reaction front is the slowest and, therefore, it defines the time period for CAL. The temperature at the outlet of the reactor (Fig. 3(c)) is almost constant for some time during the initiation of CAL since the heat released by the exothermic CuO reduction reaction fully satisfies the heat required to drive both $CaCO_3$ calcination and NiO reduction. When the sorbent is fully regenerated (see dotted blue line at t = 270 s in Fig. 3(b)), the outlet temperature slightly increases. However, due both to the small amount of reacting gas (30% CH_4) in the feed and the heat demand of the NiO reduction reactions, a ΔT of only about 5 K is observed. Such an increase in the operating temperature, however, will not result in reactor overheating.

It is noteworthy that over this stage carbon deposition on the solid material surface can be safely neglected due to the small amount of Ni content in the solid material.

3.4 Cyclic process

Other than the stages above-discussed, additional purge stages (PSs) are required to carry out the proposed SE-SMR process. In particular, a PS between CAR and OX is needed to avoid the formation of potentially explosive O_2-H_2 gas mixtures, while PSs between OX and CAL and between CAL and CAR are needed in order to depressurise and pressurise the bed, respectively.

The schematic layout of the proposed SE-SMR process is shown in Fig. 4. Air (**C_1**) and CH_4/H_2O mixture (**C_2**) compressors are needed to reach the inlet conditions required by OX and CAR, respectively. On the basis of the outlet gas composition, a controller orders a high-temperature valve to feed the appropriate inlet gas stream according to the current stage. The outlet gas stream is sent to a diverter, from which three distinct streams are obtained, namely H_2 during CAR, N_2 over both OX and PSs, and a gas mixture of CO_2 and H_2O during CAL. Part of the N_2 obtained at the outlet of the reactor during OX is recirculated in the feed air to ensure the inlet conditions required by OX, while the remainder is used to warm up the feeding air *via* a heat exchanger (**HE_1**). Nitrogen coming from PSs is directly recirculated as the feed gas stream over such stages. The gas mixture of CO_2 and H_2O is sent to a condenser: part of the recovered CO_2 is cooled down *via* heat exchanger (**HE_2**) to the inlet temperature in order to be mixed with CH_4 at the inlet of the reactor during CAL, while the remaining part can be stored.

Using the results discussed in the previous section, a cyclic operation consisting of a sequence of reforming/CaO carbonation-purge-Cu and Ni oxidation-purge-$CaCO_3$ calcination/CuO and NiO reduction-purge stages was simulated. Simulations were extended for more than 20 cycles in order to reach regime conditions in cyclic operation. These were met after 2-3 cycles, when the difference between all the state variables at each spatial node over two successive cycles was below 10^{-6}. The period of each purge stage was fixed at 100 s, which is a suitable value for the operating conditions considered in this work [46]. Detailed boundary conditions used to simulate the cyclic process are reported in Tab. 4. Fig. 5 reports the outlet molar fractions of the gaseous species during the first 4 steps of cyclic operation of the SE-SMR. The process starts with a CAR stage (blue zones), when a mixture of steam and methane is fed to the reactor. Outlet molar fractions over such stages have the same behaviour described in Section 3.1. When the y_{H2} threshold value (85%) is detected at the outlet of the reactor, a purge stage starts (white zones). After a PS of 100 s, a mixture of air and N_2 is fed to the reactor for the subsequent OX stage (green zones), which is carried out until y_{O2} at the exit of the bed reaches the threshold value (3%). A further PS is operated before the subsequent CAL stage (yellow zones): over this stage, a mixture of methane and carbon dioxide is sent to the reactor; inlet and outlet gas molar fractions are characterised by the same trend described in Section 3.3. When the outlet CH_4 molar fraction achieves its threshold value (30%), a last purge stage is run before starting a new cycle. After 2-3 cycles, regime conditions are attained and the period of each stage approaches the following values: Π_{CAR}=558 s, Π_{OX}=1495 s, Π_{CAL}=503 s; *i.e.*, at regime the period of the entire SE-SMR cycle is $\Pi_{SE\text{-}SMR}$=2856 s, considering also the three PSs.

The performance of the proposed system was evaluated in terms of CH_4 conversion (x_{CH4}), H_2 yield (Ψ_{H2}) and H_2 purity (S_{H2}). x_{CH4} was about 95%, while Ψ_{H2} and S_{H2} were about 3.2 mol_{H2} mol_{CH4}^{-}

[1] and 90%, respectively. It is important to note that the performance of the proposed process was shown to be superior to alternative H_2 production systems. In the case of ATR, maximum Ψ_{H2} and S_{H2} of about 2.6 mol_{H2} mol_{CH4}^{-1} and 73%, respectively, can be reached, as assessed by Halabi *et al.* [47], while for CLR, values of about 0.5 mol_{H2} mol_{CH4}^{-1} and 30%, respectively, were assessed by Diglio *et al.* [7]. These processes are characterised by production of hydrogen of lower quality than from the process proposed in this work, since their main product is syngas which requires a further post-processing unit to approach the performance of the proposed SE-SMR.

Table 4 - Boundary conditions used in the simulations

CAR		**OX**		**CAL**	
T_{in}, K	1073	T_{in}, K	1073	T_{in}, K	1150
P_{in}, bar	35	P_{in}, bar	35	P_{in}, bar	1
C_{CH4in}, mol m^{-3}	65	C_{N2in}, mol m^{-3}	380	C_{CH4in}, mol m^{-3}	3
C_{H2Oin}, mol m^{-3}	327	C_{O2in}, mol m^{-3}	12	C_{CO2in}, mol m^{-3}	7
PS after CAR		**PS after OX**		**PS after CAL**	
T_{in}, K	1073	T_{in}, K	1150	T_{in}, K	1073
P_{in}, bar	35	P_{in}, bar	1	P_{in}, bar	35
C_{N2in}, mol m^{-3}	392	C_{N2in}, mol m^{-3}	10	C_{N2in}, mol m^{-3}	392

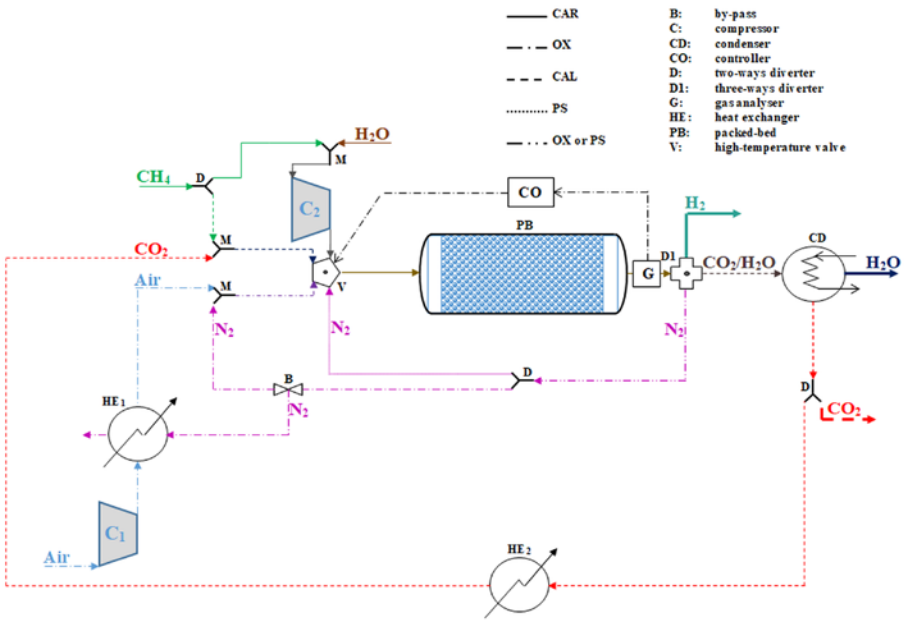

Figure 4 – Schematic layout of the proposed SE-SMR process.

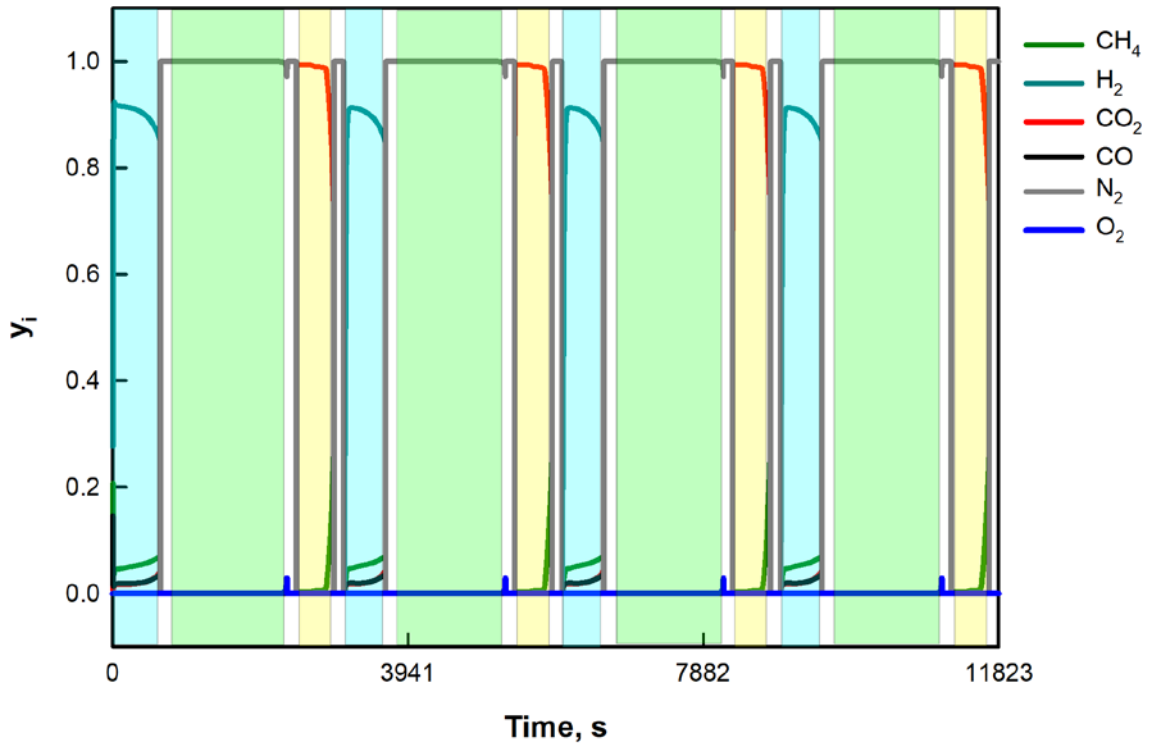

Figure 5 - Outlet gas molar fractions during multiple reforming/CaO carbonation (blue), purge (white), Cu and Ni oxidation (green) and $CaCO_3$ calcination/CuO and NiO reduction (yellow) cycles as functions of time.

3.5 Performance of reforming process

The sorbent/oxygen carrier ratio and inlet CH_4 molar fraction over the calcination stage were chosen to make the three stages of the proposed process self-sufficient from a thermal energy point of view, as suggested by Manovic and Anthony [16]. To operate the proposed process, an external heater to warm up the feed gas streams to the temperature required by each stage and power to compress the mixture of CH_4/H_2O and air fed during CAR and OX, respectively, are needed. In order both to make the process completely energy self-sufficient and to avoid CO_2 emissions due to the burning of fossil fuels, part of the hydrogen produced by the SE-SMR process can be used for such scope, as suggested by Ryden and Lyngfelt [48]. In this case, the performance of the reforming process can be evaluated by means of equivalent H_2 yield ($\psi_{H2,equiv}$), *i.e.*, the residual amount of H_2 per mole of CH_4 fed if external heat and electricity demands are covered by the produced H_2, and reforming efficiency (γ_{ref}) [49]:

$$\Psi_{H2,equiv} = \Psi_{H2} - \frac{H_{ext}}{LHV_{H2}} \quad (2)$$

$$\gamma_{ref} = \Psi_{H2,equiv} \frac{LHV_{H2}}{LHV_{CH4}} \quad (3)$$

where LHV_{H2} and LHV_{CH4} values are 241.8 kJ mol^{-1} and 802.3 kJ mol^{-1}, respectively [50]. H_{ext} represents the external heating and electricity demand of SE-SMR per mole of CH_4 supplied, calculated as:

$$H_{ext} = \frac{\left[\sum_k m_{f,k,in} \cdot cp_{f,k} \cdot \left(T_{f,k} - T_k\right)\right] + E_{el,C_1} + E_{el,C_2}}{n_{CH4,in}} = \frac{E_{th,SE-SMR} + E_{el,C_1} + E_{el,C_2}}{n_{CH4,in}} \quad (4)$$

where k=CAR, OX and CAL, $m_{f,k,in}$ is the inlet mass flow rate over stage k, $n_{CH4,in}$ is the inlet CH_4 molar flow rate, $T_{f,k}$ is the feeding temperature over stage k and T_k is the initial temperature of gas stream supplied during stage k. This value was equal to the ambient temperature (298 K) for the methane fed during CAL and to the temperature at the outlet of compressor $\mathbf{C_2}$ for the mixture of CH_4/H_2O. This latter was evaluated according to Perry and Green [50]. The power demand of compressors $\mathbf{C_1}$ ($E_{el,C1}$) and $\mathbf{C_2}$ ($E_{el,C2}$), was calculated as [51]:

$$E_{el\,i} = \left[\left(\frac{k}{k-1}\right) \cdot R_g \cdot T_{amb}\right] \cdot \left[\left(1 - \frac{P_{CAR/OX}}{P_{amb}}\right)^{\frac{k-1}{k}}\right] \cdot \left(\frac{G_i \cdot A_t}{M_i}\right) \cdot \gamma_{comp} \quad (5)$$

where i = $\mathbf{C_1}$, $\mathbf{C_2}$, the ambient temperature (T_{amb}) is 298 K, the ambient pressure (P_{amb}) is 1 bar, M_i and G_i are the molecular weight and gas flux of the gas working in the compressor i , respectively, and the compressor efficiency (γ_{comp}) is 88% [51].

Regarding the air supplied over OX, the temperature at the outlet of $\mathbf{HE_1}$ was considered as T_k (see Fig. 4). In order to evaluate this term, a standard η-NTRU model without dynamics was used to model the counter-current heat exchangers [52], by assessing the $\mathbf{HE_1}$ efficiency according to the ratio between minimum and maximum fluid thermal capacities [53].

The performance of the proposed process in terms of $\psi_{H2,equiv}$ and γ_{ref} is slightly higher than the corresponding values found in the literature for an alternative SE-SMR [13]. Equivalent H_2 yield and reforming efficiency of the proposed SE-SMR are about 2.8 mol_{H2} mol_{CH4}^{-1} and 84%, respectively, while Diglio *et al*. [13] assessed values around 2.5 mol_{H2} mol_{CH4}^{-1} and 80%, respectively.

3.6 Case study: integration with solid oxide fuel cell

In order to assess the performance of the proposed system in a real application, in this section the coupling between the developed SE-SMR and a solid oxide fuel cell (SOFC) is discussed. Since a detailed description of the SOFC operation is out of the scope of this work, a simplified modelling approach suggested in the literature [54] was adopted to evaluate the SOFC performance. Fig. 6 reports the schematic representation of the integrated system. Steam-methane mixture, air, or methane-CO_2 mixture is supplied to the SE-SMR process according to the current stage. At the system exit a stream of concentrated CO_2 during $CaCO_3$ calcination/CuO and NiO reduction stage, after condensation, and a high-purity H_2 gas stream during reforming/CaO carbonation stage are produced, respectively. In order to continuously feed H_2 to the fuel cell, hydrogen is collected into a buffer. H_2 mass flow rate at the buffer exit is equal to β ($=\Pi_{CAR}/\Pi_{SE\text{-}SMR}$) times the inlet value (*i.e.*, the mass flow rate at the outlet of the SE-SMR during CAR). Since in the H_2 gas stream of SE-SMR process there still is a small amount of unreacted methane, an internal reformer SOFC is used. The outputs of the proposed integration are the net SOFC power generation ($E_{el,net}$), *i.e.*, the difference between total SOFC power generation ($E_{el,SOFC}$) and the SE-SMR process power demand ($E_{el,SE\text{-}SMR}$) to run compressors $\mathbf{C_1}$ and $\mathbf{C_2}$, and the net SOFC heat generation ($E_{th,net}$), *i.e.*, the difference between the heat available from the SOFC ($E_{th,SOFC}$), net to the heat demand of the SOFC internal reforming process and the heat required to warm up the feed gas streams ($E_{th,SE\text{-}SMR}$).

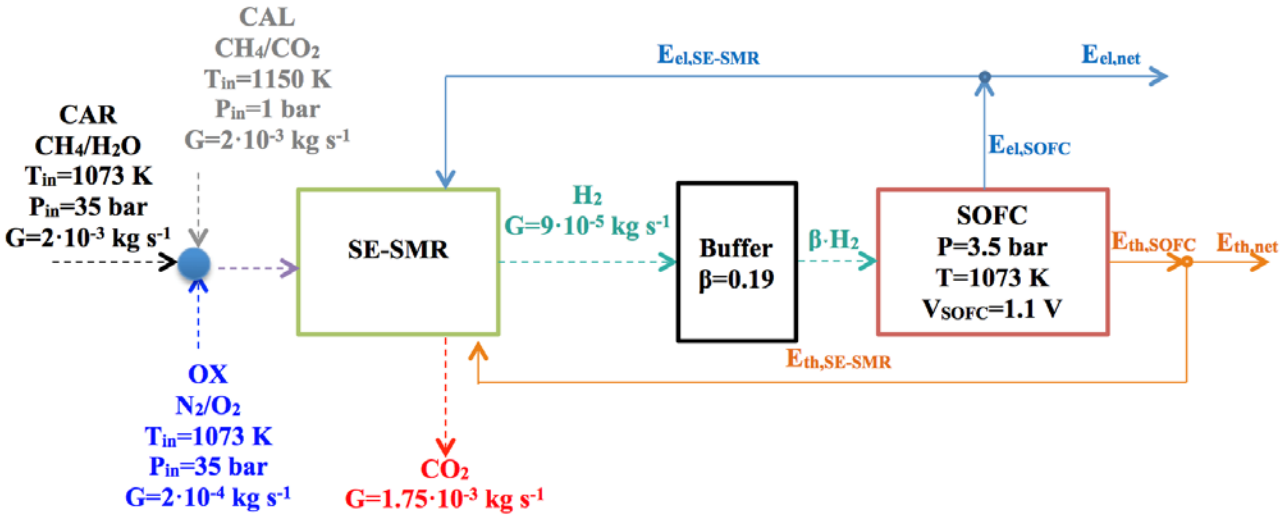

Figure 6 - Schematic representation of the integration of the proposed SE-SMR and SOFC.

The SOFC voltage was assessed through the Nernst equation [54]:

$$V_{SOFC} = \gamma_{inv}\left[\frac{-\Delta G_f^0}{2F} + \frac{R_g T}{4F} ln\left(\frac{P}{P_0}\right)\right] - V_{loss} \quad (6)$$

where ΔG^0_f is the change in molar Gibbs free energy of formation of the overall reaction occurring in the considered fuel cell ($2H_2 + O_2 \rightarrow 2H_2O$) at standard pressure ($-237.2 \cdot 10^3$ J mol^{-1}) [54], P is the operating pressure of the fuel cell (35 bar in this case), P_0 is the standard pressure, F is the Faraday constant, and V_{loss} is the fuel cell voltage loss and includes the activation-related loss, the ohmic loss and the concentration loss [55]. The voltage loss depends on several parameters, such as operating temperature and pressure, gas concentrations, current density, *etc*. Its evaluation would necessitate a detailed SOFC mathematical model, which is beyond the scope of the present article. For the sake of simplicity, V_{loss} was empirically evaluated equal to 0.2 V using the data reported by Akkaya [56] for the operating pressure and temperature utilised in the present work. The efficiency of the commercial inverter required to convert direct current from the fuel cell to alternating current (γ_{inv}) was set equal to 98% [57]. The alternating current power ($E_{el,SOFC}$), electrical efficiency (γ_{SOFC}) at the outlet of the SOFC, and new net SOFC power generation ($E_{el,net}$), were evaluated as:

$$E_{el,SOFC} = V_{SOFC} \cdot \beta \cdot \left(fu \cdot n_{H_2,SE-SMR} + 3n_{CH_4,SE-SMR}\right) \cdot 2F \quad (7)$$

$$\gamma_{SOFC} = \frac{E_{el,SOFC}}{\beta \cdot \left(n_{H_2,SE-SMR} \cdot LHV_{H_2} + 3n_{CH_4,SE-SMR} \cdot LHV_{CH_4}\right)} \quad (8)$$

$$E_{el,net} = E_{el,SOFC} - E_{el,C_1} - E_{el,C_2} \quad (9)$$

where $n_{H2,SE-SMR}$ is the molar flow rate at the outlet of the SE-SMR during CAR, net of the H_2 molar flow rate sent to the burner for heat generation; $3 \cdot n_{CH4,SE-SMR}$ is the molar flow rate of H_2 produced by internal reforming, taking into account that the steam methane reforming reaction occurs (reaction R1 in Tab. 1); and fu is the SOFC fuel utilisation factor, set equal to 0.95 [54]. Note that, for the sake of simplicity, it was considered that all CH_4 in the feed gas stream is converted in the internal reforming process, thus fu is referred only to H_2 as fuel.

The net SOFC heat generation ($E_{th,net}$) was assessed as:

$$E_{th,net} = E_{th,SOFC} - E_{th,SE-SMR} = \left[\left(\frac{\left(1-\gamma_{SOFC}\right)}{\gamma_{SOFC}} \cdot \frac{E_{SOFC}}{\gamma_{inv}}\right) - \left(\beta \cdot 3n_{CH_4,SE-SMR} \cdot \Delta H_{R1}\right)\right] - E_{th,SE-SMR} \quad (10)$$

where the second term within the square brackets on the right-hand side of Eq. (10) represents the heat demand for SOFC internal reforming.

The results of the above analysis are reported in Tab. 5. The net electric and thermal power generation of the proposed layout are about 11 kW ($E_{el,net}$) and 6 kW ($E_{th,net}$), respectively. The SOFC electrical efficiency is around 60% (γ_{SOFC}), which is very close to literature values [58]. With respect to the chemical energy of the methane at the inlet of the SE-SMR process, the net electrical ($\gamma_{el,SE\text{-}SMR\text{-}SOFC}$) and thermal ($\gamma_{el,SE\text{-}SMR\text{-}SOFC}$) efficiencies of the entire system are about 56% and 30%, respectively; *i.e.*, considering the total power generation ($E_{tot}=E_{el,net}+E_{th,net}$), the net overall efficiency of the system ($\gamma_{tot,SE\text{-}SMR\text{-}SOFC}$) is about 86%. The value of $\gamma_{el,SE\text{-}SMR\text{-}SOFC}$ is similar to those of applications reported in the literature. For example, Isfahani and Sedaghat [57] estimated an electrical efficiency of about 51.4% for a system consisting of a reformer, three fluidised bed reactors operating under chemical looping reforming conditions, a SOFC and a micro gas turbine; while Franzoni *et al*. [59] assessed an electrical efficiency of about 60% for the integration of SOFC and a gas turbine.

Table 5 - Performance of the integration of the proposed SE-SMR and SOFC.

Alternating current SOFC power generation, $E_{el,SOFC}$	15 kW
Net SOFC power generation, $E_{el,net}$	11 kW
Heat available from the SOFC, $E_{th,SOFC}$	8 kW
Net SOFC heat generation, $E_{th,net}$	6 kW
SOFC electrical efficiency, γ_{SOFC}	60%
Entire system electrical efficiency, $\gamma_{el,SE\text{-}SMR\text{-}SOFC}$	56%
Entire system thermal efficiency, $\gamma_{th,SE\text{-}SMR\text{-}SOFC}$	30%
Entire system overall efficiency, $\gamma_{tot,SE\text{-}SMR\text{-}SOFC}$	86%

The proposed process could thus be used as a near-zero-CO_2 emissions high-efficiency cogeneration system to meet both electric and thermal energy demands of a small district of residential houses.

3.6.1 Energy and environmental analysis of case study

In order to evaluate the potential of the proposed integration, a comparison between the energy and environmental performance for the present system *vs*. several conventional ones is reported. Three conventional systems, shown in Fig. 7, were considered: in **system #1** power demand is supplied by the electric grid (EG), while thermal energy demand is met by a natural gas-fuelled boiler (B); in **system #2** thermal energy demand is met by a natural gas-fuelled micro cogenerator (Micro Combined Heat and Power – MCHP), while power demand is supplied by both MCHP and EG; in s**ystem #3** thermal energy demand is met by an electric heat pump (EHP), whose primary energy demand is covered by EG that also supplies power demand.

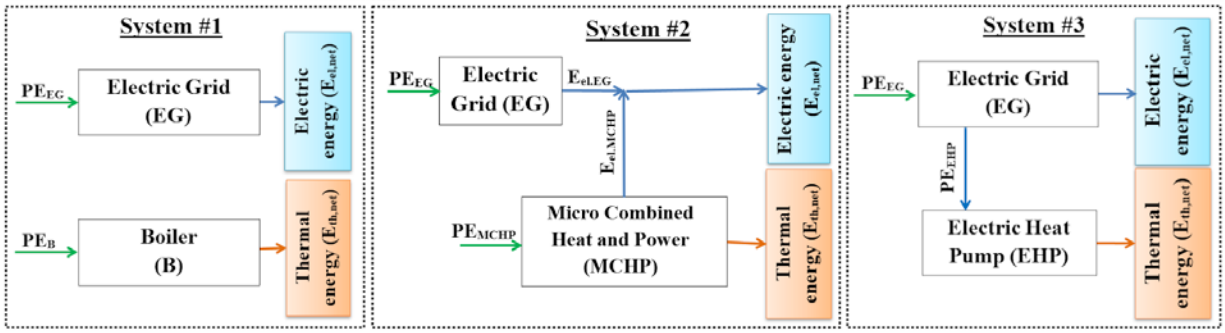

Figure 7 - Conventional systems considered in this work for benchmarking.

Taking into account the heat efficiency of the entire process, the energy consumption was evaluated by means of the fuel energy saving ratio (FESR), whose mathematical description is reported in Appendix A.1 in detail.

The proposed layout is a near-zero-CO_2 emissions system since the only source of CO_2 emissions is the small amount in the outlet gas stream over the purge stages (y_{CO2}=0.01) and at the outlet of the SOFC (when OSMR also occurs simultaneously with SMR, (y_{CO2}=0.005)). For the sake of simplicity, it was, therefore, considered that the CO_2 emissions of the proposed system are negligible with respect to those of conventional systems. The results of energy and environmental analyses are shown in Tab. 7 in terms of primary energy input, and in Fig. 8 in terms of FESR (a) and CO_{2equiv} (b).

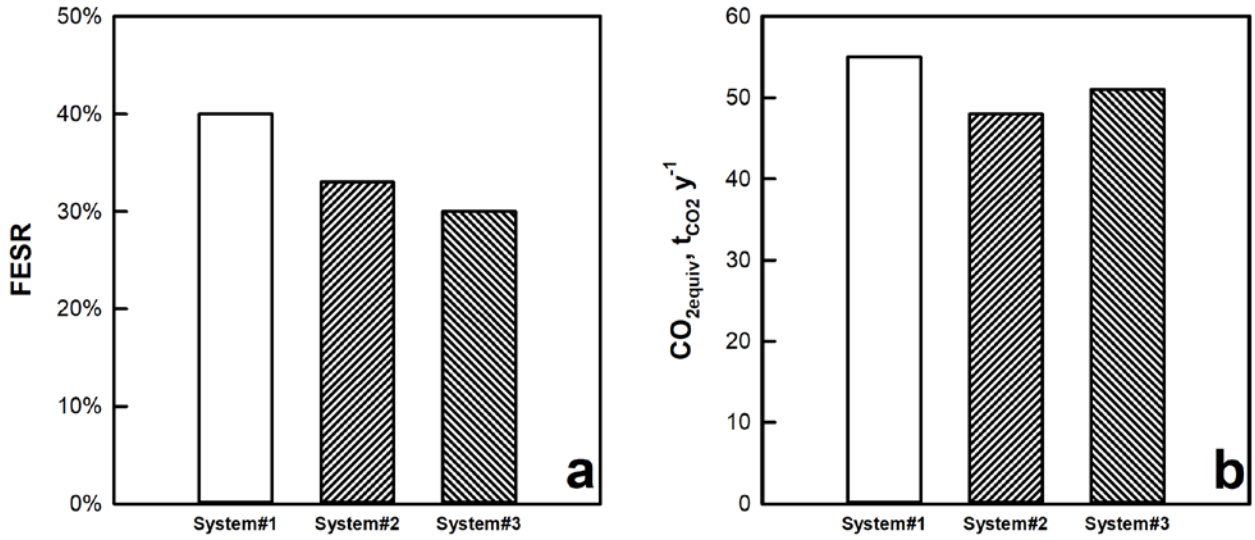

Figure 8 - Fuel Energy Saving Ratio (a) and equivalent CO_2 emissions (b).

Table 6 - Primary energy input per annum.

System#1	
Primary energy input electric grid, PE_{EG}	188.9 MWh
Primary energy input boiler, PE_B	45.5 MWh
System#2	
Primary energy input electric grid, PE_{EG}	141.8 MWh
Primary energy input cogenerator, PE_{MCHP}	68.8 MWh
System#3	
Primary energy input electric grid, PE_{EG}	201.8 MWh
Proposed System	
Primary energy input proposed system, PE_{ps}	141.6 MWh

The proposed system is characterised by better energy and environmental performance than those of all conventional systems considered in this article. In particular, both the maximum saving of primary energy (≈40%) and the maximum equivalent CO_2 emissions avoided (≈55 t_{CO2} y^{-1}) are reached with respect to **system#1**, due to the resulting low global efficiency of coupling the electric grid and a natural gas-fuelled boiler. Accordingly, the lowest FESR (≈30%) is evaluated with respect

to **system#3** since in this case thermal energy demand is supplied with a high-efficiency EHP, and the best environmental performance ($CO_{2equiv} \approx 48\ t_{CO2}\ y^{-1}$) is achieved with respect to **system#2**, characterised by the lowest primary energy demand supplied by the electric grid among all the considered conventional systems (see Tab. 7), thus by the lowest equivalent CO_2 emissions.

3.6.2 Economic analysis of case study.

The detailed cost analysis of proposed and conventional systems is reported in Appendix A.2. Results of the economic analysis are shown in Tab. 9. The proposed system is more expensive than reference ones. At worst, an additional investment about 400% higher than the investment cost of the reference system was estimated (see **system#1**). This is mainly due to the SOFC, which accounts for about 65% of the total capital requirement. **System#1** and **system#3** are very cheap because of the relatively low specific cost of the boiler and EHP, respectively. Due to the investment cost of MCHP, **system#2** is the most expensive among all considered conventional systems. The operating costs are mainly due to fuel consumption for all systems investigated. The proposed system is characterised by the highest overall efficiency, thus also by the lowest operating cost. **System#1** shows the highest operating costs since it is characterised by the highest primary energy requirement (see Tab. 7). The operating costs of **system#3** are quite close to those of **system#1** since in both cases the primary energy demand is mainly met by the electric grid. By analysing Tab. 9 it can be inferred that the pay-back period of the investment required by the proposed system is 2.0, 2.2 and 2.1 years with respect to **system#1**, **system#2** and **system#3**, respectively.

Table 7 - Results of economic analysis.

Total capital requirement **system#1**, $TCR_{cs,system\#1}$	830 €
Total capital requirement **system#2**, $TCR_{cs,system\#2}$	7,065 €
Total capital requirement **system#3**, $TCR_{cs,system\#3}$	920 €
Total capital requirement proposed system, TCR_{ps}	33,001 €
Operating costs **system#1**, $OC_{cs,system\#1}$	20,884 € y^{-1}
Operating costs **system#2**, $OC_{cs,system\#2}$	16,472 € y^{-1}
Operating costs **system#3**, $OC_{cs,system\#3}$	20,530 € y^{-1}
Operating costs proposed system, OC_{ps}	4,363 € y^{-1}

To compare the economics of the proposed system with competing cogeneration technologies, the levelised cost of electricity (LCOE), heat (LCOH) and total power (LCOTP) and the cost of CO_2 avoided (AC) were evaluated. as [60,61]:

$$\begin{cases} LCOE_{ps} = \dfrac{TCR_{ps} \cdot FCF + OC_{ps}}{CF \cdot E_{el,net} \cdot h} \\ LCOH_{ps} = \dfrac{TCR_{ps} \cdot FCF + OC_{ps}}{CF \cdot E_{th,net} \cdot h} \\ LCOTP_{i} = \dfrac{TCR_{i} \cdot FCF + OC_{i}}{CF \cdot E_{tot} \cdot h} \\ AC_{j} = \dfrac{LCOTP_{ps} - LCOTP_{j}}{\left(\dfrac{C_{O_{2equiv,j}}}{h \cdot CF \cdot E_{tot}} \right) - e_{CO_2,ps}} \end{cases} \quad (11)$$

where *i*=**ps**, **system#1**, **system#2**, **system#3** and *j*=**system#1**, **system#2**, **system#3**. The fixed and variable operating costs (*OC*) already include the cost of fuel consumption. The fixed charge factor (*FCF*) was evaluated according to Hanak *et al*. [62], considering a project interest rate and amortisation years of 8.78% and 25, respectively.

The $LCOE_{ps}$, $LCOH_{ps}$, and $LCOTP_{ps}$ of the proposed system are about 0.096 € kWh^{-1}, 0.19 € kWh^{-1}, and 0.065 € kWh^{-1}, respectively. *LCOE* is similar to that reported by Nizetic *et al*. [63], which estimated a levelised cost of energy between 0.09 € kWh^{-1} and 0.16 € kWh^{-1} for a small-size SOFC cogeneration system for residential application. Also, it should be remarked that $LCOE_{ps}$ is competitive with the average grid electricity price (UP_{ee}). Instead, due to the relatively low net thermal efficiency of the proposed system, the cost of heat is very high. Therefore, if the proposed system is mainly considered for thermal energy generation, it would require incentives to successfully compete against the reference systems. With reference to the total power generation, the proposed system is highly competitive when compared to the reference systems. Indeed, since it is characterised by the highest overall efficiency among the systems analysed, $LCOTP_{ps}$ is only about 38%, 45% and 36% of *LCTOP* of **system#1**, **system#2** and **system#3**, respectively. However, it should be considered that *LCOTP* largely depends on how the total power supplied by the system is distributed between the electricity and heat demand. Thus, it can be inferred that the proposed system represents

the best choice among the alternatives examined in this paper when the ratio between power and energy demand of the users is very high.

Since $LCOTP_{ps}$ is lower than those of the conventional systems analysed in this paper ($LCOTP_j$), the cost of CO_2 avoided (AC_j) was negative. This means that CO_2 emissions are avoided at no cost. Thus, the proposed system could be an attractive alternative for cost-effective CO_2 mitigation.

4. Conclusions

In this work Sorption-Enhanced Steam Methane Reforming (SE-SMR) in an adiabatic fixed bed using CaO/CuO/Al_2O_3(NiO) as solid material was numerically studied by means of a 1D pseudo-homogeneous numerical model. The proposed process was divided into three main stages, namely i) CaO carbonation/reforming, ii) Cu and Ni oxidation and iii) $CaCO_3$ calcination/CuO and NiO reduction. A controller automatically dictated the switch between each stage.

In detail, the first stage was carried out at high pressure (35 bar) as long as a hydrogen outlet molar fraction close to the threshold value of 0.85 was reached, in order to produce a high-purity H_2 stream. In the second stage, an oxygen-nitrogen mixture with an O_2 molar fraction of 3% at the same pressure of the previous stage was fed to the reactor by recirculating a portion of N_2 leaving the bed, in order to avoid excessive overheating of the fixed bed, to enhance the kinetics of Cu oxidation reaction, and to avoid $CaCO_3$ calcination. When the O_2 outlet molar fraction reached its feeding value, both Cu and Ni content in the solid material were fully oxidised; thus, the controller dictated the end of this stage. The last stage was operated at atmospheric pressure to enhance the kinetics of the $CaCO_3$ calcination reaction, whilst a mixture of 30% CH_4 and 70% CO_2 was fed to the reactor. This stage was operated until the outlet CH_4 molar fraction reached its inlet value, so that both Cu and Ni in the solid material were fully oxidised and the heat released by CuO reduction reaction matched the amount required by endothermic $CaCO_3$ calcination and NiO reduction. Under the above conditions, a methane conversion of about 95%, a H_2 yield of about 3.2 mol_{H2} mol_{CH4}^{-1}, and a H_2 purity around 90% were determined by means of numerical simulations for the cyclic process. Besides, a stream of concentrated CO_2 ready for storage was obtained. When a portion of produced H_2 was used to make the process energetically self-sufficient, an equivalent H_2 yield and reforming efficiency of about 2.8 mol_{H2} mol_{CH4}^{-1} and 84% were achieved, respectively.

The proposed process was integrated with a solid oxide fuel cell to assess its performance as a near-zero-CO_2 emissions cogeneration system for a small district of residential houses. Net power and thermal energy generation of about 11 kW and 6 kW, respectively, were reached. With respect

to the chemical energy of the methane at the inlet of the SE-SMR process, the net electrical and thermal efficiencies of the considered process are 56% and 30%, respectively, which means an overall efficiency of the entire system of 86%. The energy, environmental and economic performances of the proposed cogeneration system were compared with those of conventional systems, namely the electric grid coupled to a natural gas-fuelled boiler (**system #1**), electric grid coupled to a natural gas-fuelled micro cogenerator (**system #2**) and electric grid coupled to an electric heat pump (**system #3**). The analysis showed that, with respect to **system #1**, **system #2** and **system #3**, the proposed system is characterised by primary energy saving of about 40%, 33% and 30% and equivalent CO_2 emissions avoided of about 55 $t_{CO2}\ y^{-1}$, 48 $t_{CO2}\ y^{-1}$, and 53 $t_{CO2}\ y^{-1}$, respectively. The economic analysis revealed that the proposed system ensures the lowest operating cost compared to the conventional systems, with an investment pay-back period around 2.0, 2.2, and 2.1 years with respect to **system #1**, **system #2**, and **system #3**, respectively. The levelised cost of electricity (*LCOE*), of heat (*LCOH*) and total power (*LCOTP*) of the proposed system are about 0.096 € kWh^{-1}, 0.19 € kWh^{-1}, and 0.065 € kWh^{-1}, respectively, while the CO_2 emissions are avoided at no cost.

5. Appendix A

A.1 Energy and Environmental Analysis

The energy consumption was evaluated by means of the fuel energy saving ratio (FESR), defined as [64]:

$$FESR = 1 - \frac{PE_{SE-SMR-SOFC}}{PE_{cs,system\#i}} \tag{A.1}$$

The primary energy input per annum to the proposed system ($PE_{SE\text{-}SMR\text{-}SOFC}$) and to conventional systems ($PE_{cs,system\#i}$) were calculated from the following equations:

$$\begin{cases} PE_{SE-SMR-SOFC} = h \cdot CF \cdot n_{CH4,in} \cdot LHV_{CH4} \\ PE_{cs,system\#1} = PE_{EG} + PE_{B} = h \cdot CF \cdot \left(\dfrac{E_{el,net}}{\gamma_{EG}} + \dfrac{E_{th,net}}{\gamma_{B}} \right) \\ PE_{cs,system\#2} = PE_{EG} + PE_{MCHP} = h \cdot CF \cdot \left(\dfrac{E_{el,EG}}{\gamma_{EG}} + \dfrac{E_{th,net}}{\gamma_{th,MCHP}} \right) \\ PE_{cs,system\#3} = PE_{EG} = h \cdot CF \cdot \left[\dfrac{E_{el,net} + \left(E_{th,net} / COP_{EHP} \right)}{\gamma_{EG}} \right] \end{cases} \quad \text{(A.2)}$$

where $n_{CH4,in}$ is the inlet CH_4 molar flow rate in the SE-SMR process, CF is the plant capacity factor, h represents the hours in a year (8760 h/y), COP_{EHP} is the coefficient of performance of EHP, γ_{EG} and γ_B are the efficiency of electric grid and boiler, respectively, while $\gamma_{el,MCHP}$ and $\gamma_{th,MCHP}$ are the electric and thermal efficiency of MCHP, respectively.

Equivalent CO_2 emissions per annum of the conventional systems were calculated as follows:

$$\begin{cases} CO_{2equv,system\#1} = h \cdot CF \cdot E_{el,net} \cdot \mu_{EG} + PE_{B} \cdot \mu_{NG} \\ CO_{2equv,system\#2} = h \cdot CF \cdot E_{el,EG} \cdot \mu_{EG} + PE_{MCHP} \cdot \mu_{NG} \\ CO_{2equv,system\#3} = h \cdot CF \cdot \mu_{EG} \cdot \left[E_{el,net} + \left(E_{th,net} / COP_{EHP} \right) \right] \end{cases} \quad \text{(A.3)}$$

where μ_{EG} and μ_{NG} represent the specific CO_2 emissions due to electricity drawn from the grid and for natural gas consumption, respectively.

The parameters used for energy and environmental analysis are reported in Tab. A.1.

Table A.8 - Parameters used for energy and environmental analysis.

Parameter	**Value**	**Ref.**
Capacity factor, *CF*	0.80	[65]
Efficiency of electric grid, γ_{EG}	0.42	[64]
Efficiency of boiler, γ_B	0.85	[66]
Electric efficiency of MCHP, $\gamma_{el,MCHP}$	0.288	[66]
Thermal efficiency of MCHP, $\gamma_{th,MCHP}$	0.562	[66]

Coefficient of performance EHP, COP_{EHP}	3	[67]
Electirc grid specific emission factor, μ_{EG}	0.573 kg_{CO2} kWh^{-1}	[64]
Natural gas specific emission factor, μ_{NG}	0.207 kg_{CO2} kWh^{-1}	[64]

A.2 Economic Analysis

The total capital requirement for the proposed system (TCR_{ps}) was assessed as:

$$TCR_{ps} = IC_r + IC_V + IC_{sol} + IC_{aux} \tag{A.4}$$

The reactor consists of an internal refractory, a steel vessel and external refractory. Thus, the investment cost of the reactor (IC_r) accounts for the cost of both steel and refractory, which is required to protect the steel vessel at the highest temperature reached during the SE-SMR process:

$$IC_r = Vol_{steel}\rho_{steel}sc_{steel} + Vol_{refr}\rho_{refr}sc_{refr} \tag{A.5}$$

where the density of steel (ρ_{steel}) and refractory (ρ_{refr}) are 7850 kg m^{-3} [41] and 480 kg m^{-3} [68], respectively.

To evaluate the volume of steel (Vol_{steel}) and refractory (Vol_{refr}), the thickness of the steel vessel (s_s) and of refractory (s_{refr}) were required. The former was evaluated by means of the energy balance on the insulation material around the reactor wall and Fourier's law, while the latter was calculated based on a s_s/s_{refr} ratio of 0.1 [68]:

$$E_w = \frac{2\pi\lambda}{ln\left(d_a/d_r\right)}\left(T_{SE-SMR} - T_{steel}\right) \tag{A.6}$$

$$s_s = \frac{P_{SE-SMR}d_a}{4f - 1.2P_{CAR}} \tag{A.7}$$

where the maximum temperature of the steel (T_{steel}) is set to 573 K, the thermal conductivity of refractory (λ) is 0.2 W m^{-1} K^{-1} and f is $8.5 \cdot 10^{-4}$ bar [68].

The investment cost of the high-temperature valve (IC_V) was assessed according to the following economy-of-scale equation [68]:

$$IC_V = IC_{refer}\left(\frac{Q}{Q_0}\right)^{06} \tag{A.8}$$

where IC_{ref} is the reference cost of the high-temperature valve (=150,000 € [68]) and Q_0 is the reference volumetric flow rate (= 2 m^3 s^{-1}).

The investment cost of solid material (IC_{sol}) was evaluated as:

$$IC_{sol} = w_{CaO} M_{sol} SC_{CaO} + w_{Cu} M_{sol} SC_{Cu} + w_{Ni} M_{sol} SC_{Ni} + w_{Al_2O_3(NiO)} M_{sol} SC_{Al_2O_3(NiO)} \tag{A.9}$$

The investment cost of auxiliaries (IC_{aux}) comprises the cost of compressors **C1** and **C2**, of heat exchangers **HE** and **HE1**, of condenser, and of buffer. The cost of compressors (IC_{comp}) was evaluated according to [69]:

$$IC_{comp,i} = \frac{71.1\left(G_i A_i\right)}{0.9 - \gamma_{comp}} \frac{P_{CAR/OX}}{P_{amm}} ln\left(\frac{P_{CAR/OX}}{P_{amb}}\right) \tag{A.10}$$

where i = **C1**, **C2**.

The investment cost of shell-and-tube heat exchangers and condenser ($IC_{HE/cond}$) mainly depends on the required heat transfer area, according to Eqs. (A.11- A.12) [70]:

$$IC_{HE/cond} = A_{HE/cond} \cdot sc_{HE/cond} \tag{A.11}$$

$$A_{HE/cond} = n_{u,HE/cond} \cdot \pi \cdot d_{HE/cond} \cdot L_{HE/cond} \tag{A.12}$$

The investment cost of the hydrogen buffer (IC_{buffer}) considers the gas buffer and the manufacture of the storage (insulation materials, control systems and tank):

$$IC_{buffer} = (1-\beta)\cdot\left(\frac{G_{CAR}\cdot A_r}{\rho_g}\right)\cdot \Pi_{SE-SMR}\cdot sc_{buffer} \tag{A.13}$$

The investment cost of the fuel cell (IC_{SOFC}) was evaluated according to Arsalis [70]:

$$IC_{SOFC} = IC_{stack} + IC_{inv} + IC_{aux} \tag{A.14}$$

where IC_{stack} is the cost of the fuel cell stack, IC_{inv} is the cost of the inverter and IC_{aux} represents the cost of the fuel cell auxiliaries, such as internal reformer, mixers and by-pass valves. This latter was assumed to be 5% of IC_{stack} [70]. The cost of the SOFC stack was evaluated according to the active area and the operating temperature of the fuel cell, while that for the inverter was estimated by considering the power generated by the SOFC [70]:

$$IC_{stack} = \left(n_{u,cells}\pi d_{cell}L_{cell}\right)\left(296T_{SE-SMR} - 1907\right) \tag{A.15}$$

$$IC_{inv} = 10^5\left(\frac{E_{el,SOFC}}{500}\right)^{0.70} \tag{A.16}$$

The geometric parameters used for the SOFC economic analysis were taken from the literature [71] on the basis of the power generated by the SOFC.

The total capital requirement for conventional systems ($TCR_{cs,system\#i}$) was estimated as:

$$TCR_{cs,system\#i} = \sum_n E_{n,system\#i}\cdot sc_{n,system\#i} \tag{A.17}$$

where *n* is B for **system#1**, MCHP for **system#2** and EHP for **system#3**, while $E_{n,system\#i}$ is the input power of component *n* in the **system#i**.

The fixed and variable operating costs of conventional systems ($OC_{system\#i}$) and that of the proposed system (OC_{ps}) are evaluated as:

$$\begin{cases} OC_{cs,system\#1} = PE_B UP_{NG} + PE_{EG} UP_{ee} + h \cdot CF \cdot MC_B \\ OC_{cs,system\#2} = PE_{MCHP} UP_{NG} + PE_{EG} UP_{ee} + h \cdot CF \cdot MC_{MCHP} \\ OC_{cs,system\#3} = PE_{EG} UP_{ee} + h \cdot CF \cdot MC_{EHP} \\ OC_{ps} = PE_{ps} UP_{CH_4} + MC_{ps} + \left[\frac{3600 \cdot h \cdot CF}{H_{CH_4}} \right] CO_{2,SE-SMR} \cdot CTS \end{cases} \quad \text{(A.18)}$$

The parameters used for the economic analysis are reported in Tab. A.2.

Table A.9 – Parameters used for the economic analysis.

Geometric parameters for heat exchangers/condenser		
Number of heat exchanger/condenser tubes, $n_{u,HE/cond}$	25	[70]
Diameter of heat exchanger/condenser tube, $d_{HE/cond}$	0.01 m	[70]
Length of heat exchanger/condenser tube, $L_{HE/cond}$	3.35 m	[70]
Geometric parameters for SOFC		
Number of cells, $n_{u,cells}$	576	[71]
Diameter of cell, d_{cell}	0.0118 m	[71]
Length of cell, L_{cell}	0.5 m	[71]
Economic parameters		
Specific cost of steel, sc_{steel}	0.50 € kg^{-1}	[72]
Specific cost of refractory, sc_{refr}	0.45 € kg^{-1}	[72]
Specific cost of sorbent, sc_{CaO}	0.02 € kg^{-1}	[73]
Specific cost of oxygen carrier, sc_{Cu}	6 € kg^{-1}	[73]
Specific cost of catalyst, sc_{Ni}	50 € kg^{-1}	[72]
Specific cost of inert, $sc_{Al2O3(NiO)}$	1 € kg^{-1}	[73]
Specific cost of heat exchanger/condenser, $sc_{HE/cond}$	241 € m^{-2}	[70]
Specific cost of hydrogen buffer, sc_{buffer}	1,200 € m^{-3}	[74]
Specific cost of boiler, sc_B	150 € kW^{-1}	[75]
Specific cost of MCHP, sc_{MCHP}	2,500 € kW^{-1}	[65]
Specific cost of EHP, sc_{EHP}	500 € kW^{-1}	[75]
Unit price of natural gas, UP_{NG}	0.013 € kWh^{-1}	[76]
Unit price of methane, UP_{CH4}	0.019 € kWh^{-1}	[76]
Unit price of electric energy, UP_{ee}	0.1 € kWh^{-1}	[77]
Maintenance cost of boiler, M_B	0.20 € h^{-1}	[75]
Maintenance cost of MCHP, M_{MCHP}	0.20 € h^{-1}	[75]
Maintenance cost of EHP, M_{EHP}	0.05 € h^{-1}	[75]
Maintenance cost of the proposed system, M_{ps}	2% of TCR_{ps} per annum	[76]
CO_2 transport and storage cost, *CTS*	82 € t_{CO2}^{-1}	[78]

References

[1] IEA. CO_2 emissions from fuel combustion, Highlights, IEA/OECD, Paris, 2017.

[2] IEA. Key world energy statistics, IEA/OECD, Paris, 2017.

[3] IEA. World Energy Outlook, IEA/OECD, Paris, 2015.

[4] G. Marban and T. Valdes-Solis. Towards the hydrogen economy?, *International Journal of Hydrogen Energy 32 (**2007**) 1625-1637*.

[5] G. Diglio, P. Bareschino, E. Mancusi, F. Pepe. Novel quasi-autothermal hydrogen production process in a fixed-bed using a chemical looping approach: A numerical study, *International Journal of Hydrogen Energy 42 (**2017**) 15010-15023*.

[6] I. Dincer and C. Acar. Review and evaluation of hydrogen production methods for better sustainability, *International Journal of Hydrogen Energy 40 (**2015**) 11094-11111*.

[7] G. Diglio, P. Bareschino, E. Mancusi, F. Pepe. Simulation of hydrogen production through chemical looping reforming process in a packed-bed reactor, *Chemical Engineering Research and Design 105 (**2016**) 137-151*.

[8] S. Noorman, M. van Sint Annaland, H. Kuipers. Packed bed reactor technology for chemical-looping combustion, *Industrial Engineering Chemistry Research 46 (**2007**) 4212-4220*.

[9] V. Spallina, B. Marinello, F. Gallucci, M.C. Romano, M. van Sint Annaland. Chemical Looping Reforming in packed-bed reactors: modelling, experimental validation and large-scale design, *Fuel Process Technology 156 (**2017**) 156-170*.

[10] D.P. Hanak, E.J. Anthony, V. Manovic. A review of developments in pilot plant testing and modelling of calcium looping process for CO_2 capture from power generation systems, *Energy & Environmental Science 8 (**2015**) 2199-2249*.

[11] A. Perejon, L.M. Romeo, Y. Lara, P. Lisbona, A. Martinez, J.M. Valverde. The Calcium-Looping technology for CO_2 capture: On the important roles of energy integration and sorbent behavior, *Applied Energy 162 (**2016**) 787-807*.

[12] M. Broda, V. Manovic, Q. Imtiaz, A.M. Kierzkowska, E.J. Anthony, C.R. Muller. High-purity hydrogen via the sorption-enhanced steam methane reforming reaction over a synthetic CaO-based sorbent and a Ni catalyst, *Environmental Science & Technology 47 (**2013**) 6007-6014*.

[13] G. Diglio, D.P. Hanak, P. Bareschino, F. Pepe, F. Montagnaro, V. Manovic. Modelling of sorption-enhanced steam methane reforming in a fixed bed reactor network integrated with fuel cell, *Applied Energy 210 (**2018**) 1-15*.

[14] A. Antzara, E. Heracleous, A.A. Lemonidou. Energy efficient sorption enhanced-chemical looping methane reforming process for high-purity H2 production: Experimental proof-of-concept, *Applied Energy 180 (**2016**) 457-471*.

[15] L. Barelli, G. Bidini, F. Gallorini. SE-SR with sorbents based on calcium aluminates: Process optimization, *Applied Energy 143 (**2015**) 110-118*.

[16] V. Manovic and E.J. Anthony. CaO-based pellets with oxygen carriers and catalysts, *Energy & Fuels, 25 (**2011**) 4846-4853*.

[17] C. Qin, B. Feng, J. Yin, J. Ran, L. Zhang, V. Manovic. Matching of kinetics of $CaCO_3$ decomposition and CuO reduction with CH_4 in Ca-Cu chemical looping, *Chemical Engineering Journal 262 (**2015**) 665-675*.

[18] J.R. Fernandez, J.M. Alcaron, J.C. Abanades. Investigation of a fixed-bed reactor for the calcination of $CaCO_3$ by the simultaneous reduction of CuO with a fuel gas, *Industrial & Engineering Chemistry Research 55 (**2016**) 5128-5132*.

[19] L. Tan, C. Qin, Z. Zhang, J. Ran, V. Manovic. Compatibility of NiO/CuO in Ca-Cu Chemical Looping for High-purity H_2 production with CO_2 capture, *Energy Technology 6 (**2018**) 1-12*.

[20] L. Diez-Martin, I. Martinez, G. Grasa, R. Murillo. Investigation of the reduction kinetics of high loaded CuO-based materials suitable for the Ca/Cu looping process, *Fuel 230 (**2018**) 376-389*.

[21] M.A. San Pio, F. Gallucci, I. Roghair, M. van Sint Annaland. Gas-solid kinetics of CuO/Al_2O_3 as an oxygen carrier for high-pressure chemical looping processes: the influence of the total pressure, *International Journal of Hydrogen Energy 42(17) (**2017**) 12111-12121*.

[22] M.A. San Pio, F. Sabatino, F. Gallucci, M. van Sint Annaland. Importance of spinel reaction kinetics in packed-bed chemical looping combustion using a CuO/Al_2O_3 oxygen carrier, *Chemical Engineering Journal 334 (**2018**) 1905-1916*.

[23] A.L. Garcia-Lario, I. Martinez, R. Murillo, G. Grasa, J.R. Fernandez, J.C. Abanades. Reduction kinetics of a high load Cu-based pellet suitable for Ca/Cu chemical loops, *Industrial Engineering Chemistry Research 52 (**2013**) 1481-1490*.

[24] J.R. Fernandez, J.C. Abadanes, G. Grasa. Modelling of sorption enhanced steam methane reforming – Part II: Simulation within a novel Ca/Cu chemical loop process for hydrogen production, *Chemical Engineering Science 84 (**2012**) 12-20*.

[25] J.M. Alcaron and J.R. Fernandez. $CaCO_3$ calcination by the simultaneous reduction of CuO in Ca/Cu chemical looping process, *Chemical Engineering Science 137 (**2015**) 254-267*.

[26] M. Martini, A. van der Berg, F. Gallucci, M. van Sint Annaland. Investigation of the process operability windows for Ca-Cu looping for hydrogen production with CO_2, *Chemical Engineering Journal 303 (**2016**) 73-88*.

[27] M. Martini, I. Martinez, M.C. Romano, P. Chiesa, F. Gallucci, M. van Sint Annaland. Increasing the carbon capture efficiency of the Ca/Cu looping process for power production with advanced schemes, *Chemical Engineering Journal 328 (**2017**) 304-319*.

[28] L. Barelli, G. Bidini, G. Cinti, F. Gallorini, M. Poniz. SOFC stack coupled with dry reforming, *Applied Energy 192 (**2017**) 498-507*.

[29] J. Xu and G.F. Froment. Methane steam reforming, methanation and water-gas shift. 1. Intrinsic kinetics, *AIChE J 35 (**1989**) 88-96*.

[30] I. Iliuta, R. Tahoces, G. Patience. Chemical-looping combustion process: kinetics and mathematical modelling, *AIChE J 56 (**2010**) 1063-1079*.

[31] N. Rodriguez, M. Alonso, J.C. Abadanes. Experimental investigation of a circulating fluidized-bed reactor to capture CO_2 with CaO, *AIChE J 157 (**2011**) 1356-1366*.

[32] E.H. Baker. The calcium oxide-carbon dioxide system in the pressure range 1-300 atmosphere, *Journal of the Chemical Society (Resumed) (**1962**) 464-470*.

[33] F. Garcia-Labiano, L.F. de Diego, J. Adanez, A. Abad, P. Gayan. Reduction and oxidation kinetics of copper-based oxygen carrier prepared by impregnation for chemical-looping combustion, *Industrial Engineering Chemistry Research 43 (**2004**) 8168-8177*.

[34] C. Dueso, M. Ortiz, A. Abad, F. Garcia-Labiano, L.F. de Diego, P. Gayan, J. Adanez. Reduction and oxidation kinetics of nickel-based oxygen-carriers for chemical-looping combustion and chemical-looping reforming, *Chemical Engineering Journal 188 (**2012**) 142-154*.

[35] R. Hurt and J. Calo. Semi-global intrinsic kinetics for char combustion modelling, *Combustion and Flame 125 (**2001**) 1138-1149*.

[36] I. Martinez, G. Grasa, R. Murillo, B. Arias, J.C. Abadanes. Kinetics of calcination of partially carbonated particles in a Ca-looping system for CO_2 capture, *Energy & Fuels 26 (**2012**) 1432-1440*.

[37] J.R. Fernandez, J.C. Abadanes, R. Murillo. Modelling of sorption enhanced steam methane reforming in an adiabatic fixed bed reactor, *Chemical Engineering Science 84 (**2012**) 1-11*.

[38] A. Antzara, E. Heracleous, A.A. Lemonidoe. Development of CaO-based mixed oxides as stable sorbents for post-combustion CO_2 capture via carbonate looping, *Energy Procedia 63 (**2014**) 2160-2169*.

[39] M.F. Edwards and J.F. Richardson. Gas dispersion in packed beds, *Chemical Engineering Science 23 (**1968**) 109-123*.

[40] S. Yagi and N. Wakao. Heat and mass transfer from wall to fluid in packed beds, *AIChE J (**1959**) 79-85*.

[41] J.R. Rostrup-Nielsen, J. Schested, J.K. Norskov. Hydrogen and synthesis gas by steam and CO_2 reforming, *Advances in Catalysis 47 (**2002**) 65-139*.

[42] L. Han, Z. Zhou, G.M. Bollas. Heterogeneous modelling of chemical-looping combustion. Part 1: Reactor model, *Chemical Engineering Science 104 (**2013**) 233-249*.

[43] G. Diglio, P. Bareschino, E. Mancusi, F. Pepe. Numerical assessment of the effects of carbon deposition and oxidation on chemical looping combustion in a packed-bed reactor, *Chemical Engineering Science 160 (**2017**) 85-95*.

[44] G. Diglio, P. Bareschino, E. Mancusi, F. Pepe. Sensitivity analysis in the design of a packed-bed reactor for a chemical looping combustion process, *Chemical Engineering Transaction 57 (**2017**) 1027-1032*.

[45] J.R. Fernandez, J.C. Abadanes, R. Murillo, G. Grasa. Conceptual design of a hydrogen production process from natural gas with CO_2 capture using a Ca-Cu chemical loop, *International Journal of Greenhouse Gas Control 6 (**2012**) 126-141*.

[46] V. Spallina, P. Chiesa, E. Martelli, F. Gallucci, M.C. Romano, G. Lozza, *et al*. Reactor design and operation strategies for a large-scale packed-bed CLC power plant with coal syngas, *International Journal of Greenhouse Gas Control 36 (**2015**) 34-50*.

[47] M.H. Halabi, M.H.J.M. de Croon, J. van der Schaaf, P.D. Cobded, J. Schouen. Modelling and analysis of autothermal reforming of methane to hydrogen in a fixed bed reformer, *Chemical Engineering Journal 137 (**2008**) 568-578*.

[48] M. Ryden and A. Lyngfelt. Hydrogen and power production with integrated CO_2 capture by chemical looping reforming, *In. Proceedings of 7th International Conference on Greenhouse Gas Control Technologies, Vancouver, **2004**, pp. 125-134*.

[49] K. Johnses, J.R. Grace, S.E.H. Elnashaie, L. Kolbeinses, D. Eriksen. Modelling of Sorption-Enhanced steam reforming in a dual fluidized bubbling bed reactor, *Industrial Engineering Chemistry Research 45 (**2006**) 4133-4144*.

[50] R. Perry and D.W. Green. Perry's chemical engineer's handbook, 7th ed., McGraw-Hill, New York, **2007**.

[51] Division of Department of Energy, Mines and resources Canada. Compressors and turbines: energy management series for industry and commerce institution (No. 14), Ottawa, **1987**.

[52] F.P. Incropera, D.P. DeWitt, T.L. Bergman, A.S. Lavine. Fundamental of heat and mass transfer, 3rd ed., John Wiley & Sons, New York, **1990**.

[53] A. Fakheri. Heat exchanger efficiency, *Journal of Heat Transfer 129 (**2007**) 1268-1276*.

[54] J. Larminie and A. Dicks. Fuel cell systems explained, John Wiley & Sons, New York, **2003**.

[55] J. Pirkandi, M. Ghassemi, M.H. Hamedi, R. Mohammadi. Electrochemical and thermodynamic modelling of a CHP system using tubular solid oxide fuel cell (SOFC-CHP), *Journal of Cleaner Production 29-30 (**2012**) 151-162*.

[56] A.V. Akkaya. Electrochemical model for performance analysis of a tubular SOFC, *International Journal of Energy Research 31 (**2007**) 79-98*.

[57] S.N.R. Isfahani and A. Sedaghat. A hybrid micro gas turbine and solid state fuel cell power plant with hydrogen production and CO_2 capture, *International Journal of Hydrogen Energy 41 (**2016**) 9490-9499*.

[58] A.B. Stambouli and E. Traversa. Solid oxide fuel cells (SOFCs): a review of an environmentally clean and efficient source of energy, *Renewable and Sustainable Energy Reviews 6 (**2002**) 433-455*.

[59] A. Franzoni, L. Magistri, A. Traverso, A.F. Massardo. Thermoeconomic analysis of pressurized hybrid SOFC systems with CO_2 separation, *Energy 33 (**2008**) 311-320*.

[60] G. Diglio, D.P. Hanak, P. Bareschino, E. Mancusi, F. Pepe, F. Montagnaro, V. Manovic. Techno-economic analysis of sorption-enhanced steam methane reforming in a fixed bed reactor network integrated with fuel cell, *Journal of Power Sources 364 (**2017**) 41-51*.

[61] A. Trendewicz and R.J. Braun. Techno-economic analysis of solid oxide fuel cell-based combined heat and power systems for biogas utilization at wastewater treatment facilities, *Journal of Power Sources 233 (**2013**) 380-392*.

[62] D.P. Hanak, D. Powell, V. Manovic. Techno-economic analysis of oxy-combustion coal-fired power plant with cryogenic oxygen storage, *Applied Energy 191 (**2017**) 193-203*.

[63] S. Nizetic, I. Tolj, A.M. Papadopoulos. Hybrid energy fuel cell based system for household applications in a Mediterranean climate, *Energy Conversion and Management 105 (**2015**) 1037-1045*.

[64] P. Bareschino, G. Diglio, F. Pepe, G. Angrisani, C. Roselli, M. Sasso. Numerical study of a MIL101 metal organic framework based desiccant cooling system for air conditioning applications, *Applied Thermal Engineering 124 (**2017**) 641-651*.

[65] B. Metz, O. Davidson, H. de Coninck, M. Loos, L. Meyer. IPCC Special report on Carbon dioxide capture and storage, Cambridge University, Cambridge, **2005**.

[66] P. Goncalves, G. Angrisani, C. Roselli, A.R. Gaspar, M. Gameiro da Silva. Comparative energy and exergy performance assessments of a microcogenerator unit in different electricity mix scenarios, *Energy Conversion and Management 73 (**2013**) 195-206*.

[67] P. Mancarella. Cogeneration systems with electric heat pumps: energy-shifting properties and equivalent plant modelling, *Energy Conversion and Management 50 (**2009**) 1991-1999*.

[68] H.P. Hamers, M.C. Romano, V. Spallina, P. Chiesa, F. Gallucci, M. van Sint Annaland. Comparison on process efficiency for CLC of syngas operated in packed bed and fluidized bed reactors, *International Journal of Greenhouse Gas Control 28 (**2014**) 65-78*.

[69] M. Gorji-Brandpy, H. Goodarzian, M. Biglari. The cost-effective analysis of gas turbine power plant, *Energy Sources, Part B 5 (**2010**) 348-358*.

[70] A. Arsalis. Thermoeconomic modelling and parametric study of hybrid SOFC-gas turbine-steam turbine power plants ranging from 1.5 to 10 MWe, *Journal of Power Sources 181 (**2008**) 313-326*.

[71] Y. Yi, A.D. Rao, J. Brouwer, G.S. Samuelsen. Fuel flexibility of an integrated 25 kW SOFC reformer system, *Journal of Power Sources 144 (**2005**) 67-76*.

[72] H.P. Hamers, M.C. Romano, V. Spallina, P. Chiesa, F. Gallucci, M. van Sint Annaland. Energy analysis of two stage packed-bed chemical looping combustion configurations for integrated gasification combined cycles, *Energy 85 (**2015**) 489-502*.

[73] P. Fennell and B. Anthony. Calcium and chemical looping technology for power generation and carbon dioxide (CO_2) capture, Elsevier, **2015**.

[74] A. Smallbone, V. Julch, E. Wardle, A.P. Roskilly. Levelised cost of storage for pumped heat energy storage in comparison with other energy storage technologies, *Energy Conversion and Management 152 (**2017**) 221-228*.

[75] S. Magnani, P. Danti, L. Pezzola. Analysis of the coupling between CHP and EHP in an office building applied to the Italian energy market, *Energy Procedia 101 (**2016**) 588-565*.

[76] G. Diglio, D.P. Hanak, P. Bareschino, E. Mancusi, F. Pepe, F. Montagnaro, V. Manovic. Techno-economic analysis of sorption-enhanced steam methane reforming in a fixed bed reactor network integrated with fuel cell, *Journal of Power Sources 364 (**2017**) 41-51*.

[77] A. Trendewicz and R.J. Braun. Techno-economic analysis of solid oxide fuel cell-based combined heat and power systems for biogas utilization at wastewater treatment facilities, *Journal of Power Sources 233 (**2013**) 380-392*.

[78] P. Singh and M. Haines. A review of existing carbon capture and storage cluster projects and future opportunities, *Energy Procedia 63 (**2014**) 7247-7260*.